Neurobiology of Disease 108 (2017) 13–28

Contents lists available at ScienceDirect

Neurobiology of Disease

journal homepage: www.elsevier.com/locate/ynbdi

Early ciliary and prominin-1 dysfunctions precede neurogenesis impairment in a mouse model of type 2 diabetes

Tomás P. Bachor [a], Jana Karbanová [b], Edgar Büttner [b], Vicente Bermúdez [a,b], Melisa Marquioni-Ramella [a], Peter Carmeliet [c,d], Denis Corbeil [b,*], Angela M. Suburo [a,*]

[a] Instituto de Investigaciones en Medicina Traslacional (IIMT), Universidad Austral-CONICET, B1629AHJ, Pilar, Argentina
[b] Tissue Engineering Laboratories, Biotechnology Center (BIOTEC) and DFG Center for Regenerative Therapies Dresden (CRTD), Technische Universität Dresden, 01307 Dresden, Germany
[c] Lab of Angiogenesis and Vascular Metabolism, Center for Cancer Biology, VIB, Leuven, Belgium
[d] Lab of Angiogenesis and Vascular Metabolism, Dept. of Oncology, KU Leuven, Leuven, Belgium

ARTICLE INFO

Article history:
Received 25 March 2017
Revised 19 June 2017
Accepted 10 July 2017
Available online 23 July 2017

Keywords:
CD133
Cilia
Diabetes
Glucose transporter
Neurogenesis
Prominin, Subventricular zone
Neurodegeneration
Streptozotocin
Nicotinamide

ABSTRACT

Diabetes mellitus (DM) is reaching epidemic conditions worldwide and increases the risk for cognition impairment and dementia. Here, we postulated that progenitors in adult neurogenic niches might be particularly vulnerable. Therefore, we evaluated the different components of the mouse subventricular zone (SVZ) during the first week after chemical induction of type 1 and type 2 diabetes-like (T1DM and T2DM) conditions. Surprisingly, only T2DM mice showed SVZ damage. The initial lesions were localized to ependymal cilia, which appeared disorientated and clumped together. In addition, they showed delocalization of the ciliary membrane protein prominin-1. Impairment of neuroprogenitor proliferation, neurogenic marker abnormalities and ectopic migration of neuroblasts were found at a later stage. To our knowledge, our data describe for the first time such an early impact of T2DM on the SVZ. This is consistent with clinical data indicating that brain damage in T2DM patients differs from that in T1DM patients.

1. Introduction

Diabetes mellitus, both type 1 and type 2 (T1DM and T2DM), are worldwide problems that have risen to pandemic conditions (Hu et al., 2015). Current estimates from the Non-Communicable Diseases (NCD) Risk Factor Collaboration indicate that age-standardized diabetes prevalence in adults has escalated in almost every country, from 108 million in 1980 to 422 million in 2014 (NCD-RisC, 2016). Understanding this disease not only requires recognition of causal factors involved in the initial metabolic disorders but also the appreciation of diabetic consequences on various target organs. We now know that both T1DM and T2DM are associated with brain changes and an increased risk of cognitive impairment and dementia (Chatterjee et al., 2016; Smolina et al., 2015). Likewise, diabetes is associated with brain atrophy and cerebrovascular disease (Biessels et al., 2014; Ramos-Rodriguez et al., 2014). Thus, the brain is now considered as a direct target organ for diabetes. Recent evidence in adult rodent models indicates that neurogenic niches may be prime targets for diabetes (Zhang et al., 2008), further suggesting that tolls imposed on adult neurogenesis could be an important factor in diabetic and other brain disorders (Bachor and Suburo, 2012; Beauquis et al., 2006).

The subventricular zone (SVZ), localized in the lateral wall of the lateral ventricles, is the largest adult neurogenic niche (Alvarez-Buylla et al., 2008; Doetsch et al., 1999). Neural stem cells (B1 cells) have an astrocyte-like phenotype and display an apical process that traverses the ependymal lining, exposing the primary cilium to the cerebrospinal fluid (CSF) (Mirzadeh et al., 2008). Encircling apical B1 cell processes, ependymal cells display motile cilia (Mirzadeh et al., 2008). The stem cell marker prominin-1 (Prom-1, CD133) – a pentaspan membrane glycoprotein – is strongly expressed in ependymal cilia as well as in primary cilia of neural stem cells (Codega et al., 2014; Dubreuil et al., 2007; Weigmann et al., 1997). B1 cells give rise to intermediate progenitors (C cells), which divide to produce neuroblasts (A cells) (Doetsch et al., 1999; Zhao et al., 2008). The latter express the microtubule-associated

Abbreviations: AUC, area under the curve; CSD, circular standard deviation; CSF, cerebrospinal fluid; CLSM, confocal laser scanning microscope; DCX, doublecortin; DM, Diabetes mellitus; Glut, glucose transporter; GFAP, glial fibrillary acidic protein; IPGTT, intraperitoneal glucose tolerance test; NA, nicotinamide; RMS, rostral migratory stream; SEM, scanning electron microscopy; STZ, streptozotocin; SVZ, subventricular zone; T1DM, type 1 diabetes-like; T2DM, type 2 diabetes-like.

* Corresponding authors.
E-mail addresses: denis.corbeil@biotec.tu-dresden.de (D. Corbeil), amsuburo@austral.edu.ar (A.M. Suburo).

Available online on ScienceDirect (www.sciencedirect.com).

http://dx.doi.org/10.1016/j.nbd.2017.07.010
0969-9961/

protein doublecortin (DCX), an essential component of the cell migration machinery (Koizumi et al., 2006). Type A cells migrate through the rostral migratory stream (RMS) into the olfactory bulb, forming different neuronal phenotypes. Quiescent Prom-1$^+$ ependymal cells could also act as neuroprogenitors upon injury, producing new olfactory bulb neurons (Coskun et al., 2008).

A well-defined SVZ is also found in humans; however, it generates striatal interneurons (Ernst et al., 2014). Remarkably, striatal alterations have been associated with cognitive impairment in T1DM (van Duinkerken et al., 2014) and T2DM patients (Yang et al., 2015), indicating that clarification of diabetic effects on the SVZ might help to understand and possibly alleviate cognition impairment in these patients.

From the diverse rodent diabetes models available, we have chosen the classical model of T1DM (group T1DM) induced by streptozotocin (STZ). This condition was compared against the non-obese model of T2DM (group T2DM) generated by STZ given after nicotinamide (NA). Quenching of STZ diabetogenic action by NA (NA + STZ) is widely known (Nakamura et al., 2006). In chemically-induced diabetes, metabolic impairment develops in a short period, allowing a unique comparison of both conditions. Three weeks after diabetes induction, subventricular cell proliferation is significantly reduced in both STZ and NA + STZ mice (Bachor et al., 2015).

Here, we investigated the early impact of STZ and NA + STZ-induced diabetes on the adult SVZ. We show that in T2DM, but not in T1DM, severe alterations of ependymal cilia developed after only 4 days of drug injections, together with alterations of ciliary Prom-1. Reduction in the expression of other neurogenesis markers, such as nestin, glial fibrillary acidic protein (GFAP), SRY (sex determining region Y)-box 2 (Sox2), and DCX occurred after ciliary alterations. DCX$^+$ neuroblasts not only decreased in the SVZ, but also appeared in ectopic sites neighboring the RMS. Experiments in cultured ependymal cells demonstrated that altered ciliary morphology was not a direct effect of the drugs used to induce diabetes or the elevated glucose concentration. Besides corroborating the susceptibility of the SVZ as a key diabetic target, our results also point to the novelty of ependymal cilia as the cellular target of T2DM. Moreover, experiments in *Prom-1* null mice showed that this protein is likely to be involved in diabetic neurogenesis impairment.

2. Materials and methods

2.1. Animals and ethical approval

Male wild type C57Bl/6 J mice (5 to 7-weeks old) were bred and cared at the School of Biomedical Sciences, Austral University, Argentina, under permits (13-13; 13-04; 13-06; 15-04) issued by the Animal Welfare Committee from the same Institution. *Prom1*$^{-/-}$ mice (congenic C57BL/6) (Zacchigna et al., 2009) were bred at the Biomedical Services Facility of the Max-Planck-Institute of Molecular Cell Biology and Genetics (MPI-CBG, Dresden), and animal experiments were performed in strict accordance with German Animal Welfare legislation. MPI-CBG holds the necessary licenses (74-9165.40-9-2000-1 and 74-9168.25-9-2001-1) for keeping laboratory animals and collecting organs and tissues, both issued by the Regierungspräsidium Dresden, Saxony. In both animal facilities, mice had unlimited access to water and food (Cooperación Extrusado, Animal Nutrition, Buenos Aires, Argentina or Harlan 2018S, Harlan Laboratories, Indianapolis, IN). They were maintained under a 12 h light: dark schedule. Littermates were randomly separated in the different experimental groups, housing a maximum of 5 animals per cage, with a minimum floor area of 700 cm^2. Investigators were not blinded to the experimental groups.

2.2. Diabetes induction

Procedures to induce T1DM and T2DM in mice have been described (Bachor et al., 2015; Nakamura et al., 2006). In the T1DM group, mice received an intraperitoneal (i.p) injection of STZ (100 mg/kg; Sigma-Aldrich) freshly diluted in 50 mM citrate buffer (pH 4.5), repeating the procedure after 2 days. In T2DM group, mice received an i.p injection of NA (120 mg/kg; Sigma-Aldrich) 15 min before STZ. Both injections were repeated after 2 days. Non-D animals received equal volumes of citrate buffer. All animals were fastened for 4 h before injections.

2.3. Primary ependymal cell cultures

Primary ependymal cells were prepared as described (Delgehyr et al., 2015). Briefly, telencephala of newborn mice (postnatal day 1 to 3, P1-3) were dissected in cold Hank's balanced salt solution (Thermo Fisher Scientific, Waltham, MA) in sterile Petri dishes. Dissected tissue was cut into small pieces, collected into 15 ml Falcon tubes, and centrifuged 5 min at 300 ×*g*. Pelleted tissue was digested with Papain Dissociation Systems Kit according to the manufacturer's instructions (Worthington Biochemical Corporation, NJ). Dissociated cells were centrifuged for 5 min at 300 ×*g*, washed in Leibowitz medium (Thermo Fisher Scientific) and plated on poly-D-lysine (40 μg/ml; Sigma-Aldrich)-coated 25 cm^2 flasks (Cellstar®, Greiner Bio-One GmbH, Frickenhausen, Germany) in Dulbecco's modified Eagle's Medium/Glutamax (DMEM/Glutamax, Thermo Fisher Scientific), 10% fetal calf serum (FCS, PAA Laboratories GmbH, Pasching, Austria) and 1% Penicillin/Streptomycin (P/S, Thermo Fisher Scientific). Acquired progenitor cells were expanded until confluence for 5 days, then re-plated on poly-D-lysine-coated coverslips in 24-well plates (Costar®, Corning Incorporated, Corning, NY) at high density (150,000 cells/20 μl DMEM/Glutamax, 10% FCS and 1% P/S medium) and allowed to adhere for 1 h at 37 °C under 5% CO_2 atmosphere. Wells were then filled up with 1 ml of the same medium and incubated for 24 h. The following day (referred to as day 0), medium was replaced for serum-free medium DMEM/Glutamax containing 11 mM glucose and 1% P/S, and cultured for 15 days, which resulted in differentiation of progenitors into ependymal cells. Media were exchanged every 2nd day.

To evaluate the effect of diabetes-inducing drugs, 15-day-differentiated ependymal cells were treated with 1 mM STZ dissolved in 50 mM citrate buffer (pH 4.5) or 10 mM NA dissolved in water or with combination of both. In the latter case, NA was added 15 min before STZ, mimicking the in vivo procedure. Treatment was repeated after 2 days and media were exchanged for drug-free ones after another 2 days. Control cells received only citrate buffer or remained untreated. Cells were analyzed after 6 days from 1st treatment. To evaluate the effect of different concentration of glucose, 15-day-differentiated ependymal cells were further cultured in serum-free medium containing 11, 25 and 50 mM glucose, and analyzed after 7–8 days.

2.4. Blood glucose measurement

Blood glucose (BG) was measured using a small blood drop from the tail vein with a OneTouch® Ultra® glucose meter (Johnson & Johnson, UK) and its reactive strips. To perform an intraperitoneal glucose tolerance test (IPGTT), mice were fastened for 6 h (Andrikopoulos et al., 2008) without water restriction. After obtaining a basal BG measure, mice received 2 g/Kg glucose (20% solution, i.p.). Post-overload BG was acquired at 15, 30 and 60 min. In preliminary experiments, IPGTTs were made to 32 control animals. All of them showed non-diabetic curves, and the average of their basal BG levels was 105 ± 7 mg/dl. IPGTTs were done on day 6, one day before termination of the experiment. Throughout our investigation, IPGTT was performed on all experimental animals. However, to rule out the glucose overload as a possible confounder, we conducted additional control experiments without the IPGTT. Under these conditions, phenotypic alterations of ependymal cells of T1DM or T2DM mice showed the same outcome.

2.5. CSF samples and glucose measurement

A cisternal puncture was performed as described before (Liu and Duff, 2008). Mice were deeply anesthetized with an i.p. mix of Ketamine (100 mg/Kg; Fada Pharma, Argentina) and Xylazine (10 mg/Kg; Richmond, Argentina). After positioning in a stereotaxic frame, the skin of the neck was shaved and a sagittal incision was made below the occiput. The subcutaneous tissue and the underlying muscles were dissected using a scalpel, reaching the cisterna magna. Immediately after collecting the sample (approximately 10–20 μl), 5 μl were used to determine the glucose level using a Wellion-Calla® glucose meter and its reactive strips (Med Trust; Marz, Austria).

2.6. Histology

On day 7 (or day 4 as indicated), mice were deeply anesthetized and perfused through the heart as described (Bachor et al., 2015). Brain and pancreas were dissected and cryoprotected in graded sucrose solutions until a 20% sucrose concentration was reached. A coronal brain matrix for mice (David Kopf Instruments, Tujunga, CA) was used to obtain slices between +1.70 and −0.80 anterior-posterior (A-P) to the bregma (Paxinos and Franklin, 2001). Brain and pancreatic samples were embedded in optimal cutting temperature compound and snap frozen in N_2-cooled isopentane. Each frozen block contained diabetic (T1DM and T2DM) and Non-D materials to ensure similar staining intensity for experimental comparisons. Serial cryosections (10-μm thickness) obtained with a Microm HM500 OM cryostat were mounted on Superfrost™ Plus glass slides (Thermo Scientific) and stored at −20 °C until use. The histological structures were verified using cresyl violet (not shown) or hematoxylin and eosin (H & E) staining (Sigma-Aldrich) for the brain and pancreas sections, respectively.

2.7. Immunohistochemistry

Brain and pancreas samples were dried for 60 min at room temperature (RT). After two 5 min washes in a phosphate-buffered saline solution (PBS, pH 7.4), they were dehydrated in graded ethanol solutions (70%–96%–100%) and delipidized in xylene for 3 min. Slides were rehydrated (100%–96%), and the endogenous peroxidase activity was blocked by a 20 min incubation in 96% ethanol and hydrogen peroxide (5% v/v). The rehydration process continued through 70% ethanol solution and two 5 min washes in PBS. Slides were incubated with primary antibody diluted in PBS solution containing 0.5% Triton X-100 (except for the anti-Prom-1 antibody where 0.2% saponin was used) and 0.1% bovine serum albumin (BSA) for 24 h at 4 °C. Sox2 or insulin rabbit antisera (1:1000; catalogue number #ab97959 and #ab63820, respectively, Abcam), or rat mAb anti-Prom-1 (1:500; clone 13A4, eBioscience) were applied. Slides were then incubated with appropriate biotinylated secondary antibodies (1:100; Jackson ImmunoResearch Laboratories) for 1 h at RT, followed by incubation with avidin-biotin peroxidase complex reagents (Vectastain® Elite ABC system, Vector Laboratories). Immunoreactivity signals were visualized using a nickel enhanced 3,3′-Diaminobenzidine solution. Primary antibody was omitted in negative controls.

For 5-bromo-2′deoxyuridine (BrdU) incorporation, mice received a single injection (150 mg/kg, i.p; Sigma-Aldrich), 24 h before fixation, as previously described (Bachor et al., 2015). To expose incorporated BrdU, DNA denaturalization was carried out in 2N HCl plus 5% Triton X-100 for 60 min at RT. Sections were first washed in 0.1 M sodium borate buffer (pH 8.5) and then PBS. They were then incubated with a rat antiserum anti-BrdU (1:2000; Abcam) and processed as above. All samples were observed and documented using an upright microscope Nikon E800 attached to a Nikon DN100 camera.

2.8. Immunofluorescence and confocal laser scanning microscopy

Brain sections were dried for 1 h at RT, and then treated with ice-cold methanol for 15 min at −20 °C. A commercial blocking solution (Protein Block Serum Free, Dako) was used for 30 min at RT. Ependymal cells growing on poly-D-lysine-coated glass round coverslips were washed with PBS and fixed with 4% paraformaldehyde for 30 min at RT. Cells were further washed in PBS, quenched with 50 mM NH_4Cl for 10 min, and after additional washing in PBS, they were blocked and permeabilized with blocking buffer (PBS containing 0.2% gelatin and 0.1% saponin) for 20 min.

For the immunostaining, the following primary antibodies were used; guinea pig antiserum anti-DCX (1:1000; #AB2253, Millipore), mouse mAb anti-GFAP (1:1000; #G3893, Sigma-Aldrich), mouse mAb anti-glucose transporter-1 (Glut-1) (1:200; #ab40084, Abcam), goat antiserum anti-Glut-2 (1:200; #ab111117, Abcam), mouse mAb anti-acetylated-α-tubulin (1:1000; #T6793, Sigma-Aldrich), mouse mAb anti-nestin (1:200; #ab6142, Abcam) and rat mAb anti-Prom-1 (1:100). They were diluted in 0.2% saponin, 1% BSA in PBS and incubated for 24 h at 4 °C in case of brain sections or diluted in blocking buffer and incubated for 30 min at RT in case of primary cells. As negative controls, additional brain sections or coverslips with ependymal cells were processed in parallel with omission of primary antibody. After washing, appropriate Alexa Fluor®-conjugated secondary antibodies (i.e. goat anti-mouse IgG, IgG2a or IgG2b (H + L), goat anti-guinea pig IgG (H + L), goat anti-rabbit IgG (H + L), goat anti-rat IgG (H + L), donkey anti-goat IgG (H + L) (all from Thermo Fisher)) or Cy™3-conjugated AffiniPure donkey anti-rat IgG (H + L) secondary antibody (Jackson ImmunoResearch Laboratories) were applied for 30 to 60 min at RT. Nuclei were stained with 6-diamidino-2-phenylindole (DAPI) (1 μg/ml; Life Technologies, Darmstadt, Germany). Samples were mounted in Mowiol 4-88 (Calbiochem, Darmstadt). Images were captured using a confocal laser scanning microscope (CLSM) Leica TCS SP5 (Wetzlar, Germany) with a Plan Apochromat 60 × 1.2 water- or 100 × 1.4 oil-immersion objectives to obtain image z-stacks separated by a 0.25-1–μm step. Images were processed using Leica Application Suite X, Fiji (Schindelin et al., 2012) and Adobe Illustrator software. Final images corresponded to the maximum intensity projection of a 15–25 optical sections of z-stack. Alternatively, structured illumination imaging was performed with a Carl Zeiss Axiovert 200 Apotome microscope using a Plan Apochromat 63 × 1.40 oil-immersion Ph3 objective. Images were acquired in sequential mode using a tile strategy to cover the entire region of interest with a minimum resolution of 1024 × 1204 pixels. We used Carl Zeiss ZEN software for image processing.

For the TUNEL assay, we used the FragEL DNA fragmentation kit (Calbiochem) according to the manufacturer's instructions. Briefly, brain sections were dried for 1 h at RT and then incubated with Proteinase K solution (20 μg/ml) for 20 min. Positive control slides from Non-D brain sections were incubated with DNase I (1 μg/ml) in Tris-buffered saline containing 1 mM $MgSO_4$ for 20 min at RT. Slides were washed twice and incubated with Terminal Deoxynucleotidyl Transferase (TdT) buffer for 30 min at RT. After blotting the buffer solution, slides were incubated with the Fluorescein-FragEL TdT Labeling Reaction Mix in a humidified chamber at 37 °C for 1.5 h. After two washes, slides were rinsed and mounted using the Fluorescein-FragEL Mounting Media, and analyzed using a Nikon E800 fluorescent microscope.

2.9. Scanning electron microscopy

Mice were perfused as described above using a 2% paraformaldehyde, 2.5% glutaraldehyde, 0.1 M phosphate buffer solution as fixative. Brains were stored in 70% ethanol until use. To dissect the lateral ventricles, whole brains were placed in a Petri dish filled with 70% ethanol under a dissecting microscope. Olfactory bulbs and cerebellum were removed, and hemispheres were separated. To visualize the ventricular cavity, a coronal cut was made 1.0 mm posterior to the bregma. Samples

were then dehydrated in graded ethanol solutions and processed in an Automated Critical Point Dryer (Leica Microsystems, EM CPD 300, Wetzlar, Germany). After dehydration, samples were further dissected to expose the ependymal surface of the lateral wall, mounted on metal holders and sputter-coated with platinum or gold (Sputter Coating Device SCD 050, BAL-TEC GmbH, Witten, Germany). Ependymal cells grown on coverslips were fixed in 2% glutaraldehyde for 1 h at RT and then overnight at 4 °C. Samples were then treated with 1% osmium tetroxide for 2 h on ice. After washing in PBS and distilled water, they were dehydrated in acetone solutions of increasing concentrations (25–100%) and critical point-dried. Ependymal cells were mounted on metal holders and sputter-coated with gold. Samples were examined at a 5-kV accelerating voltage in cold field emission scanning electron microscopes (JEOL JSM 7500F, Japan or Philips/FEI XL 30, Oregon, USA).

2.10. Statistical and imaging analysis

Unless otherwise stated, we used one-way ANOVA followed by Newman-Keuls Multiple Comparison or Mann-Whitney *U* test to assess statistical significance, using Graphpad Prism 6.0 (GraphPad Software, La Jolla, CA). Data represent mean ± standard deviation (SD) or standard error of the mean (SEM). $P < 0.05$ was considered statistically significant. All *n* values defined in the text refer to biological replicates unless otherwise indicated.

Circular data statistics were performed with Oriana Software (Kovach computing services, UK) using the Watson U^2 test to compare dispersion of cilia orientation. Orientation of ciliary tufts was manually measured in 20 tufts from each animal ($n = 3$ or 4). The number of free ciliary tips and their orientation were scored in an area of 30 μm^2 from each animal ($n = 3$ or 4).

For immunoreactivity quantification, images were obtained from labeled sections (4–6 per brain between +1.00 and bregma, for details see (Bachor et al., 2015)), containing the regions of interest (ROIs) around the lateral ventricle. Structured illumination (Apotome) was used, producing images free of scattered light. Single images were digitally stitched into photomontages. The lateral wall ROI included all labeled cells neighboring the ventricular wall (50 μm deep) along a 400 μm segment ventral to the dorsolateral angle of the lateral ventricle. Similar ROI's were used to score cell nuclei in the dorsal and medial walls. For cytoplasmic immunofluorescence, an arbitrary threshold value was defined to segregate positive pixels in all sections. The resulting segregated area (positive pixels only) was measured by an automatic action (Adobe Photoshop© CS6), and expressed as the ratio of segregated area to total area. DAPI$^+$, Sox2$^+$ and DCX$^+$ cells were manually scored. These results are given as the ratio of positive nuclei to DAPI$^+$ nuclei scored in each ROI.

3. Results

3.1. Animal models to study the early impact of diabetes on the adult brain

All mice showed normal fasting BG levels at the beginning of the experiment (day 0). In comparison with non-diabetic (Non-D) controls, T1DM and T2DM mice showed significant BG increases under fasting (day 6) and non-fasting conditions at the end of the experiment (day 7) (Fig. 1A, B). CSF glucose concentration was evaluated in non-fasting mice. On day 7, CSF glucose concentration in T1DM animals was significantly higher than in T2DM or Non-D mice, whereas no differences were observed between these last two groups (Fig. 1C). In the IPGTT, T1DM animals showed high fasting BG and delayed glucose reduction, while T2DM mice maintained normal fasting BG levels but failed to lower BG after 60 min of glucose overload (Fig. 1D). Thus, the area under the curve (AUC) for T2DM mice was significantly smaller than the T1DM AUC but nonetheless higher than control animals (Fig. 1E).

No gross alteration of the diabetic pancreases was detected in H & E stained-sections (Supplementary Fig. 1A). However, the area of pancreatic islets in T1DM and T2DM animals (101.0 ± 16.7 μm^2 and 123.7 ± 29.9 μm^2, respectively) was significantly lower than in Non-D mice (143.4 ± 28.6 μm^2; Non-D vs T1DM, $P < 0.0001$; Non-D vs T2DM, $P < 0.001$; 30 islets per condition; $n = 4$). Furthermore, immunohistochemistry revealed a reduction in insulin expression in T1DM mice, which was less evident in T2DM animals (Supplementary Fig. 1B). No major abnormality (e.g., hydrocephalus), changes in antero-posterior length or variations in the weight were observed in the diabetic brains (Supplementary Fig. 1C, D). Body weight was significantly lower in T1DM mice than in Non-D and T2DM animals (Supplementary Fig. 1E).

3.2. Ciliary disarray in the SVZ ependymal layer of T2DM mice

We used the antero-dorsal region of the SVZ for evaluation of the ependymal surface with scanning electron microscopy (SEM). In Non-D and T1DM animals, the majority of ciliary tufts were oriented in a common direction (Fig. 2A, B, green arrows). In T2DM mice, by contrast, ciliary tufts from adjacent cells often pointed in opposite directions (Fig. 2A, B, orange arrows). Additionally, ependymal cilia from the same tuft and from adjacent cells frequently appeared clumped together (Fig. 2A, arrowheads). In mice receiving NA without STZ, cilia were not different from those in Non-D animals (Fig. 2C). Higher magnifications confirmed that, in T2DM mice, clumping mainly occurred at ciliary tips (Fig. 2D, dashed circles).

After arbitrarily setting the mean angle to zero, we calculated the variation of tuft orientation around the mean and plotted the results in a circular histogram using Oriana software (Kovach Computing) (Fig. 2E). The circular standard deviation (CSD) confirmed the disorientation of ependymal ciliary tufts of T2DM mice in contrast to Non-D and T1DM mice ($n = 4$, $^{***}P < 0.001$, Watson U^2 test). No significant differences appeared between Non-D and T1DM mice ($P = 0.762$).

To evaluate ciliary clumping, we measured the proportion of free ciliary tips within a pre-defined area and recorded the orientation of individual cilia. As shown for ciliary tufts, most ciliary tips were orientated in the same direction in Non-D and T1DM mice, but were disorientated in T2DM (Supplementary Fig. 2A, B). In agreement with the clumping of cilia, the number of free ciliary tips in a selected area (30 μm^2) of ventricular surface was solely 87 ± 12 in T2DM brain, while an average of 131 ± 15 and 139 ± 12 ciliary tips were scored in Non-D and T1DM, respectively ($n = 4$; Non-D vs T2DM, $P < 0.001$; Non-D vs T1DM, $P = 0.645$).

3.3. Neither STZ nor NA + STZ alter the surface of ependymal cells in vitro

Since it was critical to rule out the possibility of a direct effect from the diabetes-inducing drugs in vivo, we prepared primary cultures from postnatal mice and analyzed them by SEM upon exposure to STZ (1 mM) or NA (10 mM), alone or combined, for 6 to 7 days. Interestingly, none of the drugs modified cilia architecture (Fig. 3A). In controls, about half the cilia within a given cell appeared as separate entities from each other (Fig. 3A, top panels; Supplementary Fig. 3A, B, non-adherent phenotype, 58.65 ± 13.04%; >250 cells were evaluated, $n = 4$). However, in some cells, ciliary tips were adhered to each other (Fig. 3A, bottom panels, adherent phenotype, dashed circles; Supplementary Fig. 3A, B, adherent/sticky-end phenotype, 31.18 ± 3.95%). In a minute fraction of cells, gluing of the apical ciliary segments resulted in the clumping of ciliary tufts (Supplementary Fig. 3A, B, adherent/clumped phenotype, 10.18 ± 14.91%). Exposure to STZ and/or NA did not modify the proportion of the non-adherent and adherent ciliary phenotypes and did not affect the expression or subcellular localization of Prom-1 (Fig. 3B, star), a protein selectively associated with membrane protrusions, including cilia (Corbeil et al., 2001; Dubreuil et al., 2007). Visualization with acetylated-α-tubulin labeling (Ac Tub) showed that not all cultured ependymal cilia expressed Prom-1 (Fig. 3B, arrowhead). The localization of Glut-2 also differed from cell-to-cell, being either concentrated at the base of cilium or distributed over the entire ciliary

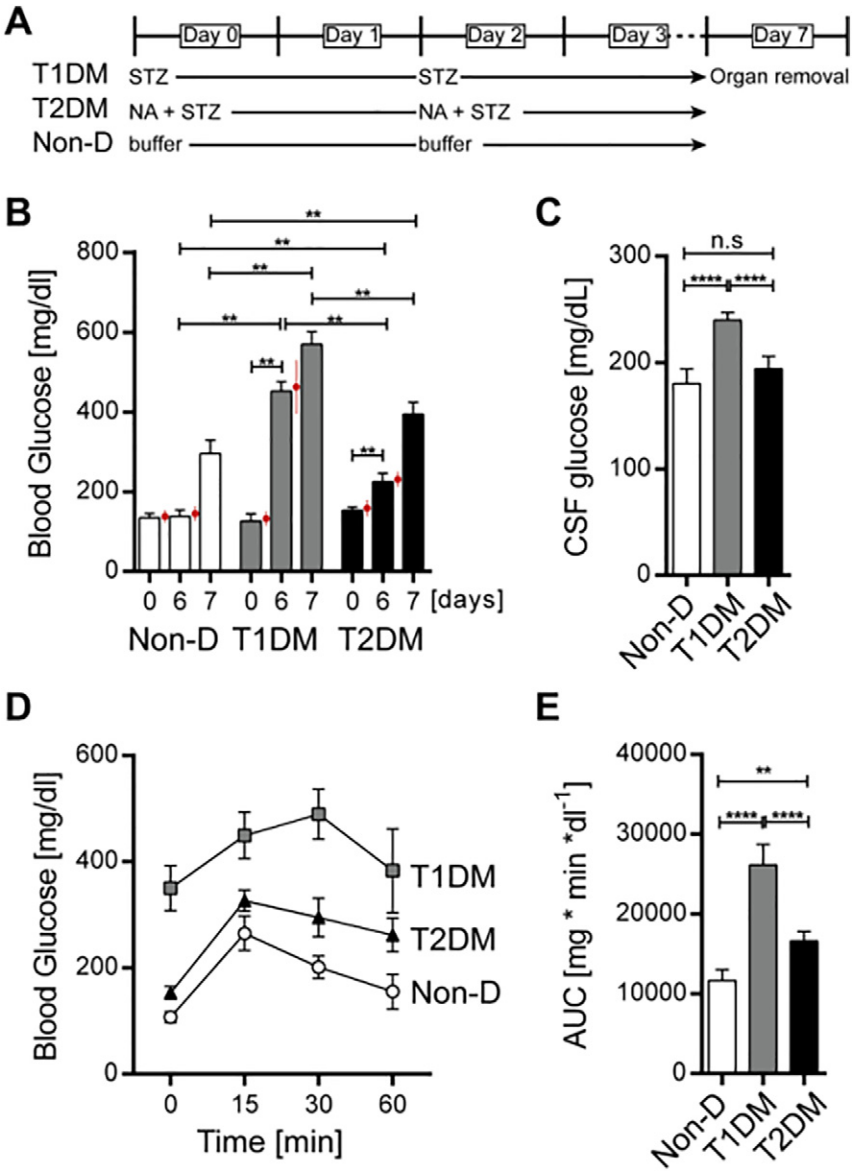

Fig. 1. Induction of diabetes-like conditions in mice alters their metabolic outcome. (A) Timeline of the protocols used in our experiments. STZ, alone or in combination with NA, was injected on day 0 and 2, and animals were euthanized at day 7. (B) BG concentrations were determined in Non-D, T1DM and T2DM mice ($n = 5$ for each groups) after 6 h fasting at day 0 (i.e. before diabetes induction), day 6, and non-fasting at day 7. Fasting values from a larger group of animals ($n = 20$, red dot and bar) were not significantly different from those shown here. (C) Glucose concentration in CSF acquired from the cisterna magna in non-fasting state at day 7. (D) Curves displaying glucose tolerance at day 6, as shown by IPGTT, in the different experimental groups ($n = 5$). (E) Comparison of the areas under the curve (AUC) for each experimental group. Data are presented as the mean ± SD. $^{**}P < 0.01$; $^{****}P < 0.0001$, one-way ANOVA; n.s., non-significant.

length (Fig. 3B, asterisk and arrow, respectively). The presence or absence of Prom-1 did not influence the subcellular localization of Glut-2, a molecular target of STZ (Fig. 3B, C). It is worth noting that, contrary to Glut-2, Glut-1 was concentrated on microvilli and absent from cilia (Fig. 3D). Exposure to STZ and/or NA did not affect the expression of both glucose transporters (Fig. 3B-D).

Differential expression of ciliary markers might reflect the presence of ependymal cells from distinct walls of the lateral ventricle, since expression of ciliary Prom-1 is greater in the SVZ ependymal cells than in other ventricular regions (Castañeda et al., 2010). Likewise, immunolabeling revealed that Glut-2 was concentrated near the base of the cilium in cells located in the ventricular lateral wall, but distributed over the entire cilium in the medial wall (Fig. 3E). The cause of this phenomenon is currently unknown, but our observations support the notion that ependymal cells in the SVZ surface have unique properties probably related to their role in neurogenesis.

3.4. The T2DM milieu induced striking changes in the SVZ neurogenic niche

Since ciliary impairment might alter neurogenesis in the SVZ (Ohata and Alvarez-Buylla, 2016), we analyzed the molecular and cellular components of this neurogenic niche (Fig. 4A), including the expression profile of neurogenesis markers. One week after drug-induced diabetes-like conditions, evaluation of neurogenesis markers Prom-1, GFAP, nestin and DCX showed critical changes in T2DM mice (Fig. 4B). We did not detect quantitative or localization changes of these neurogenesis markers in Non-D vs T1DM mice, but they were significantly reduced in T2DM brains (Fig. 4C, $^{****}P < 0.0001$; $n = 4$ for each group). In contrast, glucose transporter Glut-1, which was not reduced in T2DM, significantly increased in T1DM brains (Fig. 4C, $^{**}P < 0.01$).

We also evaluated cell proliferation using BrdU incorporation, cell number by DAPI labeling and cell death by TUNEL assays. Quantification of BrdU immunoreactivity in the lateral wall did not show any changes

in Non-D or T1DM animals, whereas T2DM mice evidenced a significant reduction indicating a decline in actively dividing cells (Fig. 4D, E; $n = 3$ for each group; $^{**}P < 0.01$). Differential scoring of DAPI-labeled cell nuclei in the lateral, dorsal, and medial walls of the lateral ventricles, showed that their number was reduced only in neurogenic niche found in the lateral wall of T2DM mice, without any changes in T1DM

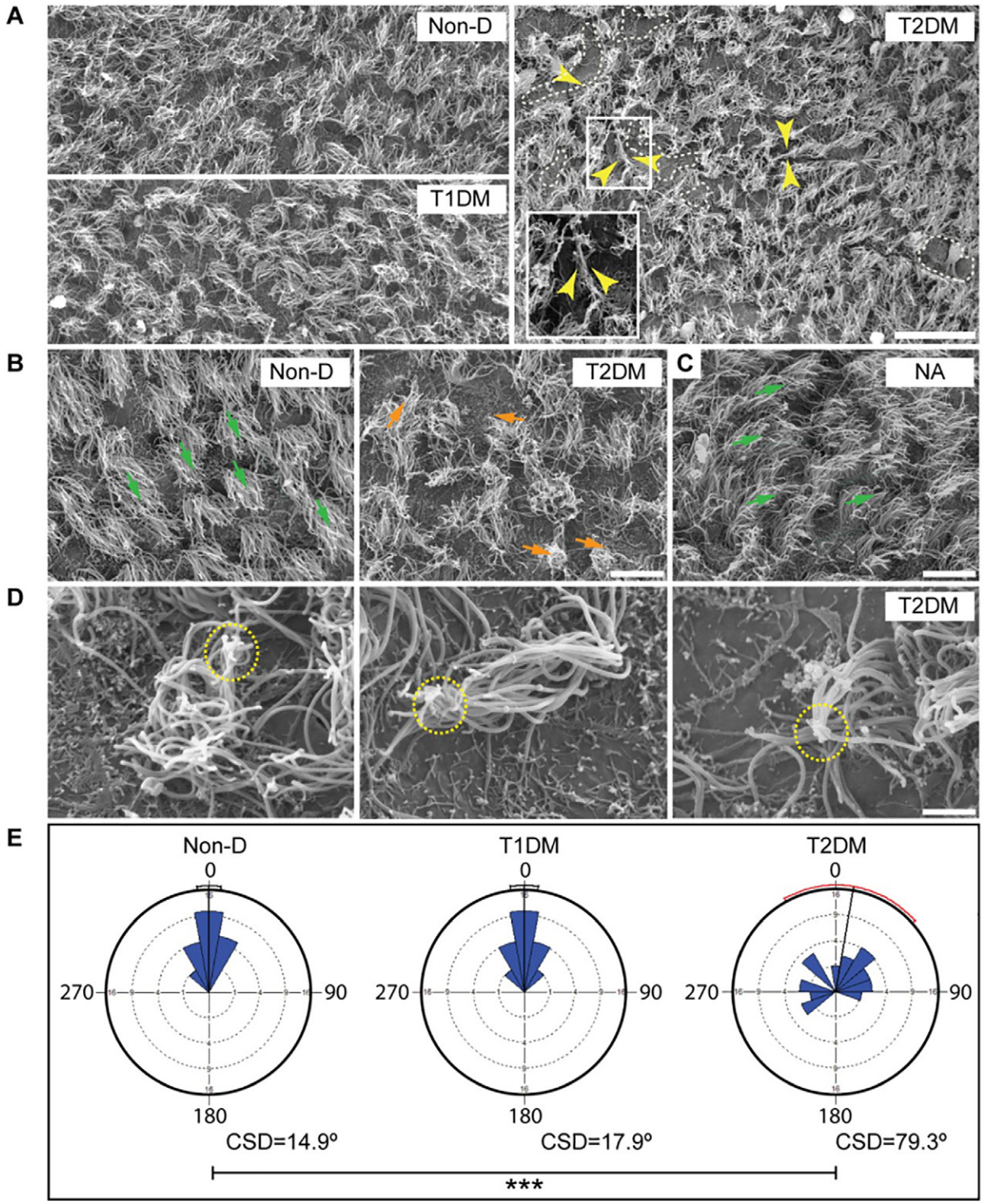

Fig. 2. Severe disorganization of the SVZ ependymal cilia in T2DM mice. (A) The ependymal cells lining the SVZ were analyzed by SEM. In Non-D and T1DM mice, ciliary tufts followed a common direction, whereas in T2DM they twisted in various directions. In addition, cilia clumped together (yellow arrows), allowing the visualization of large areas of ependymal cell surface (white dashed lines). Inset shows stuck cilia. (B) SVZ ependymal cilia from Non-D and T2DM are shown under higher magnification. Green arrows depict the common direction followed by ciliary tufts in the ependymal surface of Non-D brain. By contrast, ciliary tufts were disorientated (orange arrows) in T2DM brain. (C) The ependymal surface of an animal that received two NA injections on days 0 and 2 showed no evidence of ciliary disorganization, demonstrating that changes in T2DM cannot be explained by NA injection. (D) Higher magnification images showing individual tufts with cilia completely disorganized and collapsing at their tips (yellow dashed circles). (E) Angular distribution of vectors representing the orientation of ciliary tufts around the mean with its 95% confidence limit indicated by the arc. Each circular histogram corresponds to one animal. The lack of a common orientation of ciliary tufts in T2DM, in contrast to Non-D and T1DM mice, resulted in a high circular standard deviation (CSD) of the mean angle. Scale bars, (A) 20 μm, (B, C) 15 μm, (D) 2 μm. Data information: 4 animals were analyzed for each experimental group. $^{***}P < 0.001$ Watson U^2 test.

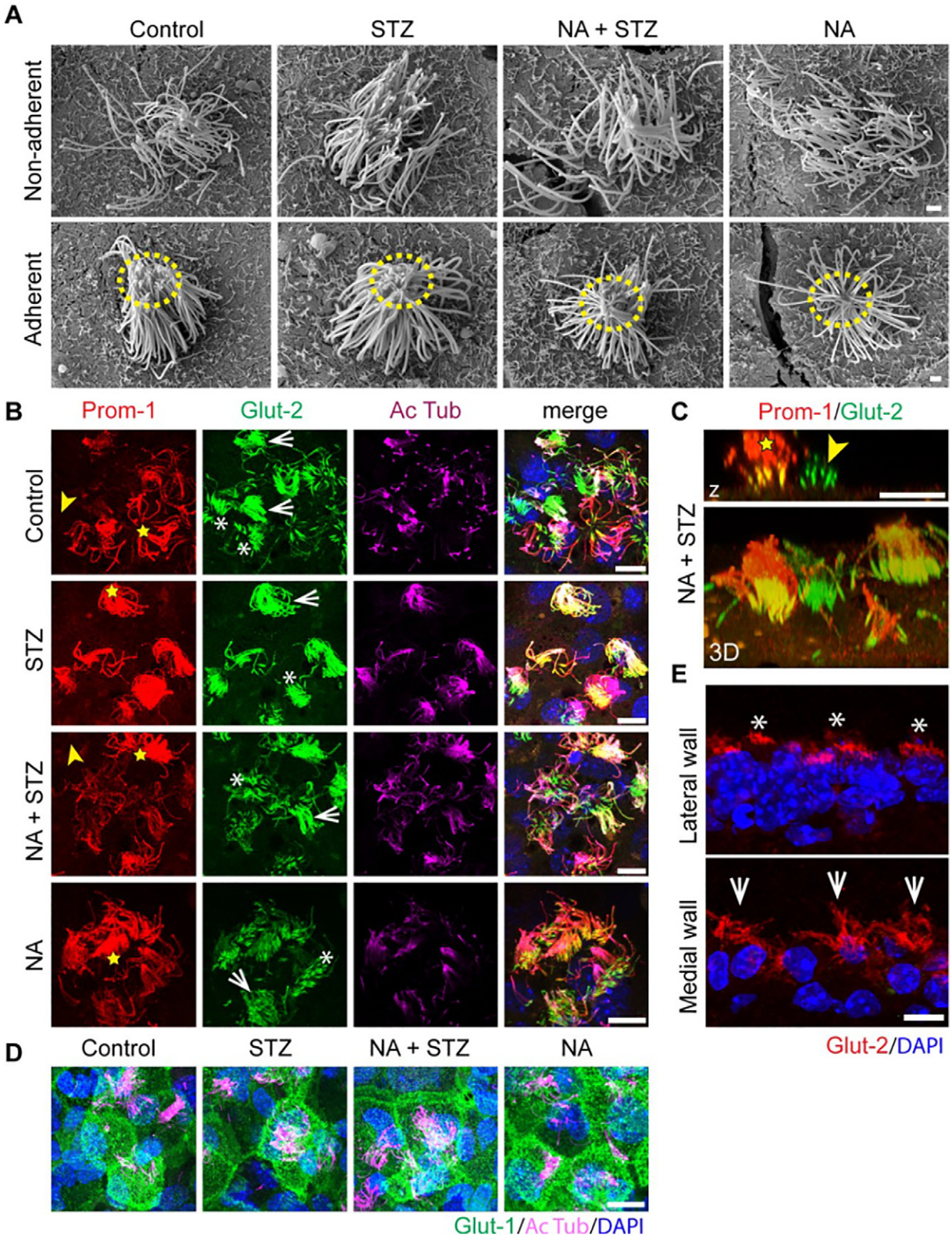

Fig. 3. No alteration of ependymal surface appeared in primary ependymal cells in the presence of STZ or NA + STZ. (A-D) Differentiated primary ependymal cells prepared from postnatal mice were cultured for 6 days in standard glucose medium (11 mM, Control) or treated with 1 mM STZ alone and/or 10 mM NA. They were subjected either to SEM (A) or immunocytochemistry (B–D). In all experimental conditions, individual cilia within a ciliary tuft remained separated from each other (A, top panels) while about 30% of cells harbored cilia with sticky-ends (A, bottom panels, dashed circles; for quantification see Supplementary Fig. 3). For CLSM studies, samples were immunolabeled for Prom-1, Glut-1, Glut-2 and Ac Tub. Nuclei were visualized with DAPI. Composites of 25 optical x-y sections (B, D) or z-section (z) and tri-dimensional (3D) reconstruction images (C) are shown. Stars and arrowheads indicate the Prom-1 positive or negative cells, respectively (B, C). Asterisks and arrows show Glut-2 concentrated at the base of cilium or distributed over its entire length (B), respectively. In contrast, Glut-1 is found in microvilli (D). The expression and subcellular localization of antigens are identical in all conditions. (E) The immunolabeling of lateral and medial walls of the lateral ventricle from adult mouse reveals the differential distribution of Glut-2 in each ventricular region. Scale bars, (A) 1 μm; (B–E) 10 μm.

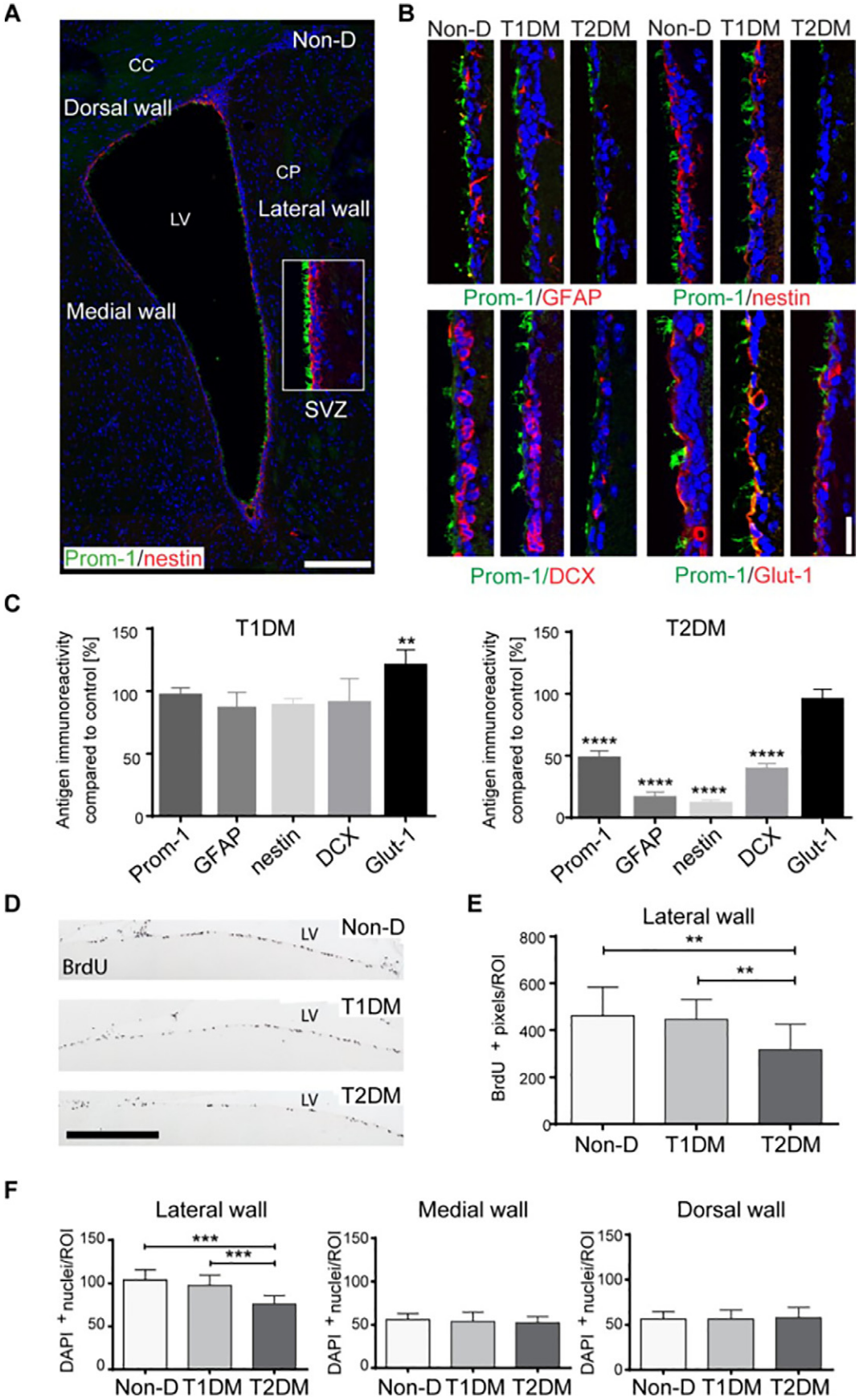
A
Non-D
CC
Dorsal wall
CP
LV
Lateral wall
Medial wall
SVZ
Prom-1/nestin
B
Non-D T1DM T2DM Non-D T1DM T2DM
Prom-1/GFAP
Prom-1/nestin
Prom-1/DCX
Prom-1/Glut-1
C
T1DM
T2DM
Antigen immunoreactivity compared to control [%]
150
100
50
0
**
****
Prom-1
GFAP
nestin
DCX
Glut-1
D
Non-D
T1DM
T2DM
LV
BrdU
E
Lateral wall
BrdU + pixels/ROI
800
600
400
200
0
**
**
Non-D
T1DM
T2DM
F
Lateral wall
Medial wall
Dorsal wall
DAPI + nuclei/ROI
150
100
50
0
***
***
Non-D T1DM T2DM

mice (Fig. 4F; Non-D vs T2DM, $^{***}P < 0.001$). DAPI labeling did not show any evidence of necrotic and/or pyknotic nuclei. Furthermore, TUNEL assays gave negative results in the SVZ of all different groups analyzed (see below). Altogether, these observations show that each diabetic condition elicited a different response at the SVZ molecular and cellular levels, with the most striking changes being found in T2DM animals.

3.5. Impact of the diabetic environment on the subcellular localization of Prom-1

Changes in Prom-1 expression in T2DM mice prompted us to analyze its subcellular localization in ependymal cells. In Non-D and T1DM mice, Prom-1 was found in almost every ependymal ciliary tuft along the ependymal surface of the SVZ (Fig. 5A). By contrast, in T2DM, ciliary tufts displayed much less Prom-1 immunoreactivity, which appeared close to the ependymal surface (Fig. 5A, dashed line). The change in Prom-1 localization evokes the collapse of ciliary tufts observed in T2DM by SEM. In addition, Prom-1 also appeared within the apical cytoplasm of ependymal cells in T1DM and T2DM, while no signs of Prom-1 internalization were found in Non-D animals (Fig. 5A, arrows).

Interestingly, double immunostaining of Prom-1 and Ac Tub revealed the absence of Prom-1 at the tips of cilia in T2DM animals (Fig. 5B). Quantification of double-labeled cilia revealed that only 11.6 ± 10.7% of cilia in T2DM contained Prom-1 at their tips, whereas this number increased to 80.3 ± 4.9% and 78.6 ± 3.7% in Non-D and T1DM mice, respectively (Fig. 5C). The reduction of Prom-1$^+$ ciliary tips in T2DM was statistically significant by comparison to Non-D and T1DM (Fig. 5C, 548, 447 and 570 cilia were evaluated in Non-D, T1DM and T2DM, respectively; $n = 3$). Thus, the T2DM condition not only reduced Prom-1 but also disturbed its subcellular localization.

3.6. Can changes in CSF glucose concentration alter prom-1 expression and ciliary organization?

As previously described, glucose concentration in T1DM mice CSF was higher than in T2DM or Non-D animals (Fig. 1C). Therefore, established ependymal cell cultures were grown for another 7–8 days in media containing 11 mM glucose, which is equivalent to the CSF glucose concentration of non-fasting Non-D mice. At this concentration, most individual cilia within a given tuft were distant from each other as observed in Non-D and T1DM mice (Supplementary Fig. 3A, B, non-adherent phenotype). A similar pattern was found when we increased the glucose concentration to 50 mM (equivalent to 900 mg/dL), which was substantially higher than the levels detected in the CSF of T1DM mice (225 mg/dL). High glucose did not affect the general organization of ciliary tufts, but induced abnormalities at the level of ciliary tips. At 11 mM glucose, tips appeared in 3 distinct forms: bulbous (bubble-tip), with a hook (hook-tip) or straight (straight-tip), in an approximately similar proportion (Supplementary Fig. 3C, D). The 50 mM glucose concentration favored the appearance of straight-tip cilia at the expense of bubble-tip ones (Supplementary Fig. 3D). However, the presence of high glucose concentration neither influenced the ciliary length nor predisposed cilia to stick to each other (Supplementary Fig. 3A–D). Indeed, we did not observe any correlation between tip phenotypes and adherence phenomena. In contrast to high glucose concentration, neither STZ and/or NA affected cilia tips (Supplementary Fig. 3E). The molecular mechanism behind the modification of ciliary tips, as well as its presence in vivo requires further investigation. Re-examination of SEM images obtained from Non-D, T1DM and T2DM animals suggested that most tips displayed bubble- or hook-tip phenotypes (see Figs. 2A–D, 6A, B and 8A). This would be consistent with the relatively low glucose concentrations (close to 11 mM) found in the CSF of Non-D and T2DM animals.

Finally, high glucose levels (25 or 50 mM) in culture media did not affect the expression of Prom-1, Glut-1 or Glut-2 (Supplementary Fig. 4A, B). Although a relationship between glucose levels and changes of ependymal cilia cannot be totally excluded, other still unknown factors may be involved in the T2DM impairment of SVZ ependymal cilia.

3.7. Ependymal cilia tend to stick to each other in Prom-1 null mice

Since *Prom-1* ablation causes a disorganization of the retinal photoreceptor outer segment, which is a modified sensory cilium (Gurudev et al., 2013; Zacchigna et al., 2009), we used *Prom-1* null mice to investigate whether the lack of Prom-1 could induce ependymal ciliary alterations like those observed in T2DM. In the SVZ ependymal layer, the absence of Prom-1 did not alter the general orientation of ciliary tufts (Fig. 6A; 80 ciliary tufts were evaluated per brain; $n = 3$ for each group) or the orientation of single cilia (Fig. 6B). Nonetheless, cilia clumped together either at their tips or all along their length (Fig. 6B, C), which resulted in a decrease of observable separate tips within a tuft. An average of 134 ± 8 tips could be scored within a 30 μm^2 ventricular area in wild type (WT) animals, while solely 82 ± 10 tips in *Prom-1* null mice ($n = 3$ for both groups; WT vs *Prom-1* null $P < 0.01$, Student's *t*-test). Thus, the presence of cilia clumping in *Prom-1* null mice supports the role of Prom-1 as one of the early diabetic targets (Fig. 6D).

No significant differences were observed in the organization of ciliary tufts and ciliary tips of ependymal cells derived from *Prom-1* null or WT mice and cultured in vitro (Supplementary Fig. 5A, B, respectively). However, *Prom-1* null cilia presented numerous small protruding structures all along their length (both at 11 and 50 mM glucose), which were more rarely observed in cells derived from WT animals (Supplementary Fig. 5B, red arrowheads). It remains to be determined whether they are budding vesicles, such as those giving rise to Prom-1-rich extracellular membrane vesicles released into the CSF (Dubreuil et al., 2007; Huttner et al., 2008; Marzesco et al., 2005), or released vesicles that adhered to cilia. The latter issue would be consistent with the increased adhesiveness observed in vivo.

3.8. Ectopic migration of neuroblasts in T2DM mice

The majority of cells in the adult SVZ are proliferating neuroblasts (Garcia-Verdugo et al., 1998). Thus, the decrease of DAPI-labeled nuclei and neurogenesis markers in the lateral ventricular wall of T2DM animals might be explained, not only by a reduction of cell proliferation, but also by increased migration through the RMS. To evaluate this issue, we analyzed DCX immunolabeling in parasagittal and coronal brain sections covering the entire RMS. We found that, in Non-D controls and diabetic models, DCX$^+$ neuroblasts were organized in a continuous chain along the RMS (Fig. 7A). In every T2DM mouse analyzed (6/6 animals), DCX$^+$ cells were also found outside the RMS, denoting ectopic migration. Misplaced cells were frequently detected in the caudoputamen (CP), nucleus accumbens (NAc) and along the olfactory peduncle (Fig. 7A, arrowheads). Coronal sections through the lateral ventricle did not show any

Fig. 4. Down regulation of neurogenic markers and proliferation in the SVZ of T2DM mice. (A-C) Brain sections of Non-D, T1DM and T2DM mice were immunolabeled for Prom-1 (green) in combination with GFAP, nestin, DCX and Glut-1 (red). Nuclei were visualized with DAPI (blue). Samples were observed under structured illumination microscopy. An overview of a coronal section through the Non-D brain, showing the dorsal, medial, and lateral walls of the lateral ventricle is displayed (A). Inset illustrates the SVZ located in the lateral wall. The co-expression of Prom-1 with other individual markers in the lateral wall is shown (B) and quantified (C). A ROI in the ventricular wall was quantified in 4 serial non-consecutive coronal sections per animal. Graphs show immunoreactivity in diabetic mice as a proportion of the Non-D control. Note that T1DM only showed an increase of Glut-1, whereas T2DM presented a large decrease of neurogenesis markers, without significant change in Glut-1. (D, E) Proliferation was reduced in T2DM brain. BrdU immunoreactivity in the lateral wall was observed by bright field microscopy (D) and quantified (E). CC, corpus callosum; CP, caudoputamen; LV, lateral ventricle. (F) Reduction of total cell number in the lateral wall of T2DM mouse. DAPI-stained nuclei were quantified along the 3 walls of the lateral ventricle. Data are presented as the mean ± S.D. 4 animals were analyzed for each experimental group. $^{**}P < 0.01$, $^{***}P < 0.001$, $^{****}P < 0.0001$, one-way ANOVA. Scale bars, (A, D) 200 μm, (B) 50 μm.

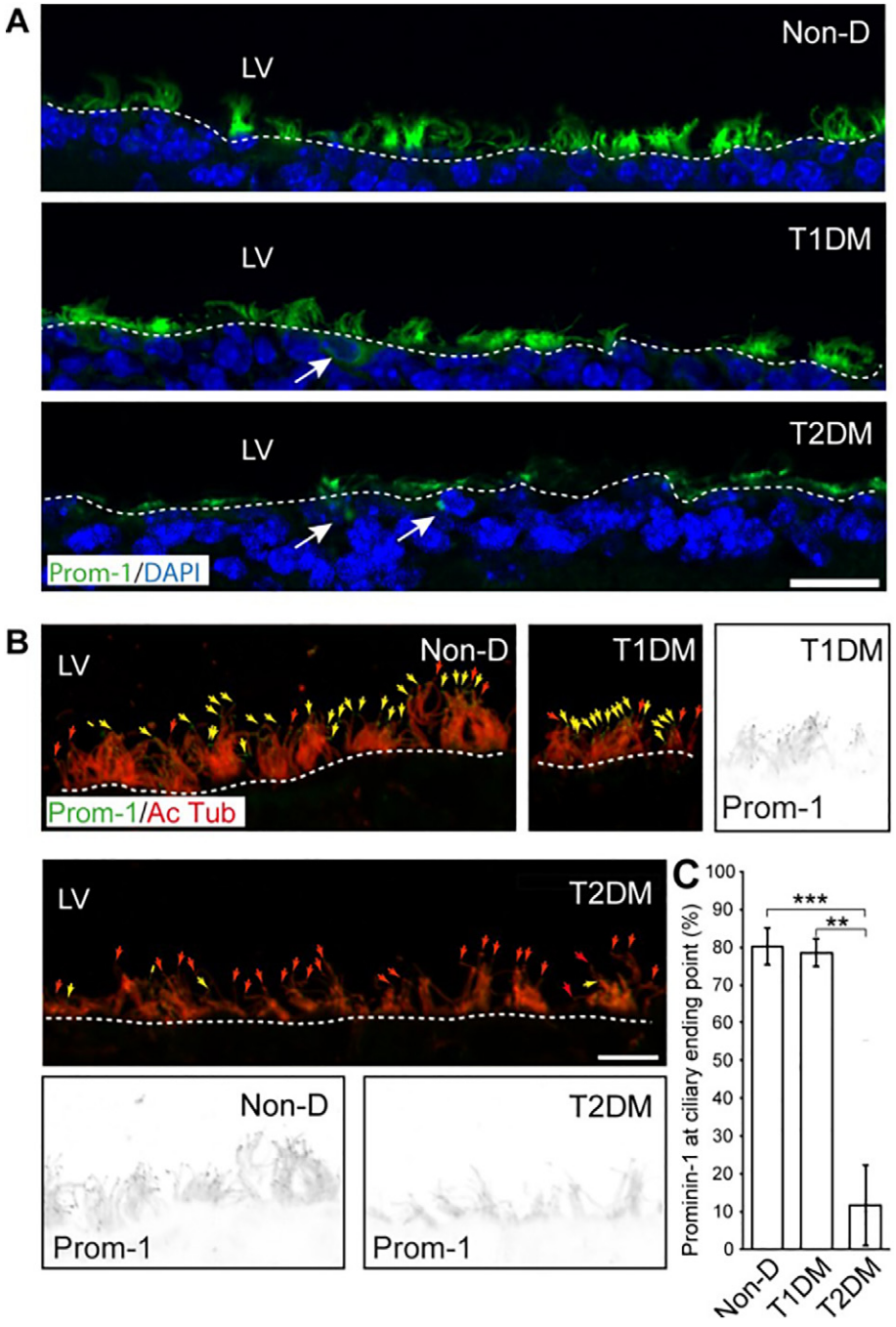

Fig. 5. Delocalization of Prom-1 at the ciliary tips of ependymal cells in T2DM mice. (A, B) Brain sections of Non-D, T1DM and T2DM mice were immunolabeled with Prom-1 (green) alone (A) or in combination with Ac Tub (B, red). Nuclei were visualized with DAPI (blue). Samples were observed by CLSM. In Non-D and T1DM mice, Prom-1 labeled whole ciliary tufts protruding from the apical membrane (dotted line) of ependymal cells into the lateral ventricle lumen. In T2DM, Prom-1 appeared closer to apical membrane, consistent with altered ciliary disorganization observed by SEM. In some cells of the two diabetic models, Prom-1 seemed to be internalized (A, white arrows). Ac Tub labeling revealed that Prom-1 was concentrated at tips of cilia in both Non-D and T1DM mice (yellow arrows), but not in T2DM (red arrows). Black-and-white images, corresponding to a single optical section in the green channel, highlight the presence of Prom-1-immunoreactivity in the ciliary tips in Non-D and T1DM or its absence in T2DM mice. (C) The appearance of Prom-1 at the ciliary tip was quantified. >400 cilia were evaluated in each condition ($n = 3$). Data are presented as the mean ± SEM. **, $P < 0.01$; ***, $P < 0.001$. LV, lateral ventricle. Scale bars, (A) 25 μm, (B) 10 μm.

out of place DCX^+ neuroblasts (Fig. 7B). Nevertheless, sections through 3 different levels of the RMS confirmed the presence of ectopic DCX^+ cells clusters within the NAc and the anterior olfactory nucleus (AON) of T2DM mice (Fig. 7C–E, arrowheads). In parasagittal sections through the RMS of T2DM animals, an average of 25 ± 3 ectopic DCX^+ cells/ROI was scored, while in Non-D and T1DM, hardly any ectopic cells were observed. A similar situation was observed in coronal sections where an average of 6 ± 1 ectopic DCX^+ cells/ROI was scored (Fig. 7F).

3.9. Ependymal cilia alterations appear earlier than changes in neurogenesis markers

The data described above prompted us to investigate potential changes in the SVZ at only 4 days after NA + STZ injection (Supplementary Fig. 6A). Both T1DM and T2DM mice showed significant BG increases under fasting (day 3) and non-fasting conditions at the end of the experiment (day 4), when compared to Non-D mice (Supplementary Fig. 6B).

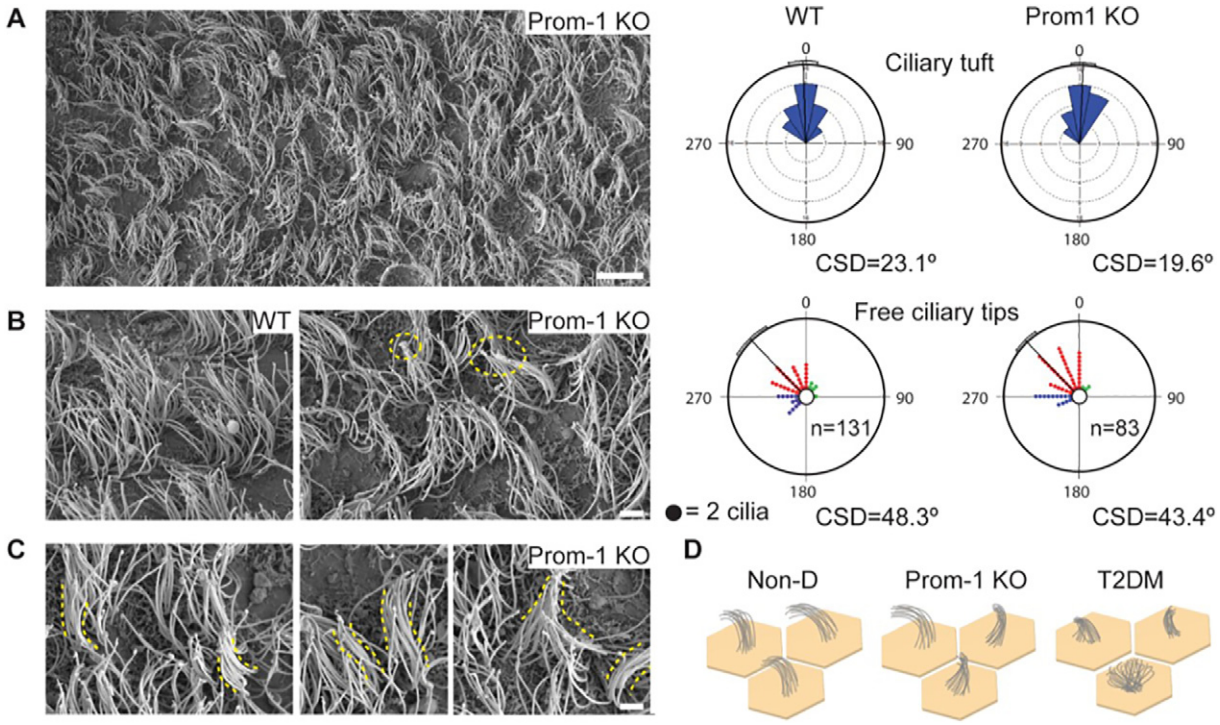

Fig. 6. The absence of Prom-1 does not alter the orientation of ciliary tufts but leads some individual cilia to clump together. (A-C) Ependymal cells lining the lateral wall of the lateral ventricle from wild type (WT) or *Prom-1* null (KO) brains were observed by SEM. In the Prom-1 KO animals, most ciliary tufts followed the same direction (A). Control ependymal cells showed separate cilia, whereas in the Prom-1 KO mouse, some ciliary tufts evidenced clumping either at the tips of the cilium (B, dashed circles) or all along their length (C, dashed lines). Nevertheless, the number of cilia (n) with an accessible tip within a 30 μm^2 area was smaller in Prom-1 KO than in WT (B). Circular standard deviation (CSD) of the mean is indicated. (D) Illustration of the typical ciliary phenotypes observed in the SVZ ependymal epithelium of Non-D, Prom-1 KO and T2DM mice. Scale bars, (A) 10 μm, (B, C) 5 μm.

Moreover, both fasting and non-fasting BG levels of T1DM mice were significantly higher than T2DM animals.

Again, SEM analysis showed a conspicuous perturbation of ependymal cilia orientation in T2DM, but not in Non-D or T1DM, animals, both at the level of ciliary tufts and individual cilia (Fig. 8A, B; $n = 3$ for each group; T1DM, data not shown). In addition to this disorientation, a significant decrease in the number of separate ciliary tips was observed in T2DM (89 ± 10 cilia per 30 μm^2 areas) by comparison to Non-D brain (135 ± 16; $n = 3$ for each group; Non-D vs T2DM, $P < 0.001$), as reported above at 7 days. No evidence of cell death was detected at this stage (Supplementary Fig. 7).

We also investigated the expression and localization of Prom-1 at the 4-day stage. Interestingly, both a significant reduction of Prom-1 and a delocalization from ciliary tips to the apical membrane surface of ependymal cells were observed in T2DM by comparison to Non-D and T1DM brains (Fig. 8C, D, green and red arrowheads, respectively). Thus, these results strongly indicate a relationship between ciliary disorganization and the expression and localization of Prom-1.

Lastly, we analyzed the expression of Sox2 and DCX. Within the adult SVZ, transcription factor Sox2 is found in GFAP$^+$ nestin$^+$ multipotential neural stem cells. Sox2 expression persists until cells differentiate, and its presence is required for maintaining neural precursor cell properties (Pevny and Nicolis, 2010). Neither Sox2 nor DCX immunoreactive cells were reduced at 4 days (Fig. 8E, F), whereas a significant decrease of Sox2 and DCX was observed at the 7-day T2DM stage (Fig. 8E, G, see also above), indicating that ciliary impairment preceded alterations of neurogenesis.

4. Discussion

Diabetes is a chronic disease, which evolves through several years, as different tissues react to metabolic damage. Although we know a great deal about the final stages of diabetic lesions, relatively little has been investigated about the earliest stages, when preventive measures might provide complete recovery. Our present study was specifically designed to search for initial damage in the SVZ of adult mice, considering that neurogenic niches are highly sensitive to the diabetic imbalance and that loss of cell renewal most likely predicts further structural and functional impairment of the niche and distant related structures. For this particular reason we chose the pharmacologically-induced diabetes models (Nakamura et al., 2006), since they allow the comparison of different diabetic conditions within the same time line.

We found that partial elimination of insulin-producing β cells, achieved by a combination of NA and STZ, with its concomitant metabolic disorders, correlated with a severe disarray of cilia in the ependymal layer lining the SVZ, appearing during the first week of the T2DM condition. Using SEM, we found that ependymal cilia became entangled and stuck to each other, particularly at their tips. Entanglement and collapse of ciliary tufts, which were often pointing in different directions, suggest alterations of ciliary movement. It has been established that the coordinated movement of motile cilia is key to facilitate circulation of CSF, allowing transportation of signaling molecules and nanovesicles, as well as detoxifying a wide variety of substances (Del Bigio, 1995; Feliciano et al., 2014). Several pathologies have been linked to defects in primary and motile cilia (Fliegauf et al., 2007), suggesting their central role in a plethora of cellular processes. Furthermore, defects in the primary cilia of pancreatic β cells were recently linked to abnormal insulin secretion and consequent T2DM development in rodents (Gerdes et al., 2014). Other tissues and organs, particularly those expressing Prom-1 such as retina (i.e. photoreceptor cells), kidney, liver and pancreas, need to be studied to ascertain whether changes observed in our T2DM model are specific to ependymal cilia.

Early damage of the SVZ in T2DM mice implies that damage of the neurogenic niche was independent of BG levels, which were much higher in T1DM than in T2DM. Besides, ciliary impairment would not be directly caused by CSF glucose concentrations, which were almost

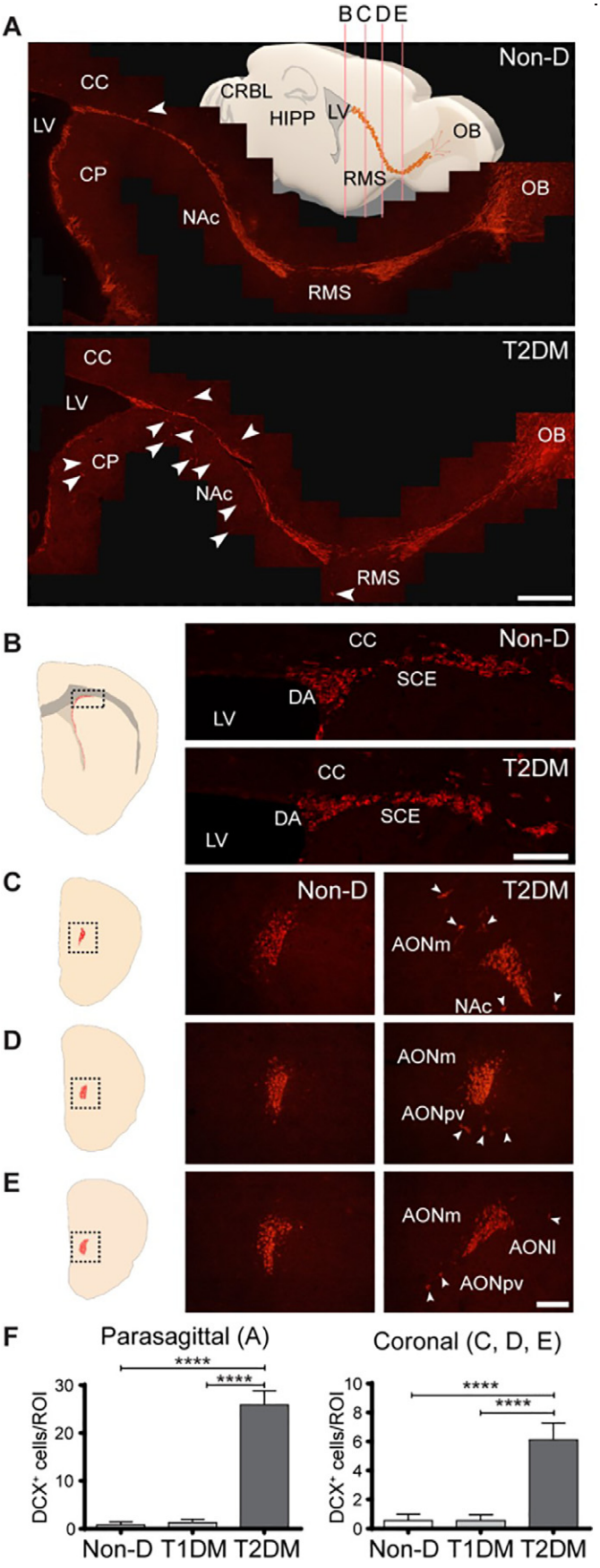

identical in non-fasting T2DM and non-diabetic mice. Furthermore, ependymal cells grown in vitro only showed alterations at the tip of individual cilia, but not on ciliary tuft organization, even when glucose concentrations were about 4 times higher than those found in the CSF of T1DM animals. Changes in the shape of the tip in ependymal cells grown in 50 mM glucose suggest that excess glucose levels in the CSF, as we have observed in T1DM mice, and is known to occur in humans (Sartorius et al., 2015), might affect intraflagellar mechanisms transporting various proteins to ciliary tips (Ishikawa and Marshall, 2017; Tran et al., 2008). However, Prom-1 traffic would not be affected in vitro, since we did not detect changes of this protein in the cilia of ependymal cells grown in 50 mM glucose.

Since the drugs used for diabetes induction and the high glucose concentration did not affect the organization of ependymal ciliary tufts in vitro, an unidentified metabolic change might be involved in T2DM ciliary impairment. This hypothesis is supported by the similarity of CSF non-fasting glucose concentrations in non-diabetic and T2DM mice. Insulin resistance has not been described in this model (Nakamura et al., 2006), and we have not found changes in insulin-dependent protein kinase B (Akt) phosphorylation in T2DM muscle (TB, MMR, unpublished experiments). However, we should explore whether selective insulin brain resistance is present in these mice (Mullins et al., 2017). At the same time, metabolic changes could induce endoplasmic reticulum stress, altering the highly regulated balance of proteins involved in intraflagellar trafficking and leading to early ciliary dysfunction (see below). On the other hand, we should also consider whether the early ependymal changes described would be found in every case of T2DM, or just in a subgroup. Although it is generally considered that a decrease in insulin sensitivity always precedes T2DM development, β-cell dysfunction significantly contributes to the pathogenesis of this disease. Moreover, recent studies indicate that impaired β-cell function is a primary underlying defect in a significant proportion of the diabetic population (Festa et al., 2006; Ohn et al., 2016). Hence, T2DM models with and without insulin resistance should be compared in future studies.

Further investigations are required to determine which biochemical factor/s present in T2DM are directly responsible for the observed ciliary phenotypes. Inflammation can affect ciliogenesis, however, the inflammatory milieu is most severely disturbed by T1DM than by T2DM (Kim et al., 2014). On the other hand, we can postulate that the acute disappearance of insulin-producing cells in T1DM might elicit strong brain replacement mechanisms (e.g., by insulin-like growth factors 1 or 2 (Ziegler et al., 2015)), which would not be equally available when a significant amount of insulin is still circulating, as in T2DM. The apparent advantage of T1DM would be rapidly lost, since proliferation in the SVZ zone niche of T1DM mice almost completely disappears after 3 weeks (Bachor et al., 2015). In line with this hypothesis, T1DM ependymal cells showed increased Glut-1 immunoreactivity, suggesting an adaptive mechanism for the uptake of excessive glucose. Conversely, in T2DM, Glut-1 immunoreactivity was not different from controls, but Prom-1 and the neurogenesis markers Sox2, GFAP, nestin and DCX were strikingly

Fig. 7. Ectopic migration of DCX$^+$ neuroblasts in T2DM mice. (A–E) Parasagittal (A) and coronal (B–E) sections taken at different levels (see cartoons) of Non-D and T2DM brain were immunolabeled for DCX (red) and observed by epifluorescence microscopy. Although no major alteration was observed in the migration pattern of DCX$^+$ cells in T2DM by comparison to Non-D mice, DCX$^+$ cell clusters were ectopically located in the corpus callosum (CC), caudoputamen (CP) and nucleus accumbens (NAc) outside the rostral migratory stream (RMS) (A, white arrowhead). Serial coronal sections revealed no ectopic DCX$^+$ cell expression in the dorsolateral angle (DA) and the subcallosal enlargement (SCE) of T2DM mice (B) while they appeared in anterior structures surrounding the RMS *en route* to olfactory bulb (OB) (C-E). (F) Quantification of DCX$^+$ cells located outside the RMS in parasagittal and coronal sections. AON, anterior olfactory nucleus (m, medial; l, lateral part; pv, posteroventral); CRBL, cerebellum; HIPP, hippocampus; LV, lateral ventricle. Data are presented as the mean ± S.D. 12.5 or 5 mm^2/section ROI were used for sagittal and coronal sections, respectively. 3 sections were analyzed per brain, $n = 3$ animals. ****$P < 0.0001$, one-way ANOVA. Scale bars, (A) 500 μm, (B) 100 μm, (C–E) 50 μm.

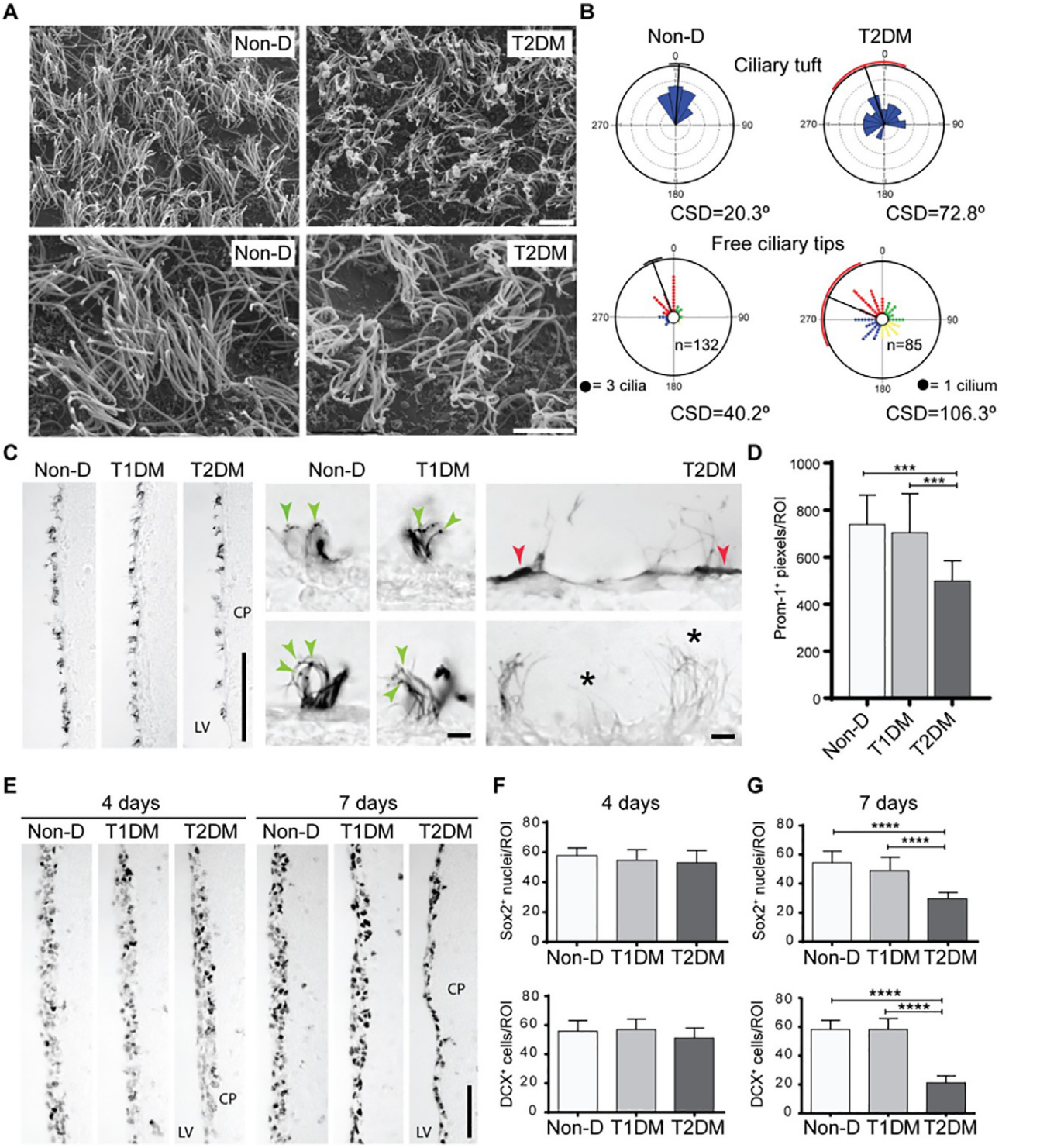

Fig. 8. Alterations in the SVZ 4 days after drug injection. (A) STZ, alone or in combination with NA, was injected on day 0 and 2, and animals were euthanized at day 4. Representative SEM images of the ependymal SVZ lining show the ordered pattern of ciliary tufts in Non-D (also found in T1DM, not shown), in comparison with the disorientation and clumping of cilia in T2DM brain. (B) Angular distribution of vectors representing the orientation of ciliary tufts or single free cilia around the mean is shown and its 95% confidence limit is indicated with the arc. 20 ciliary tufts including 85 individual cilia or more, were used to build each circular graph ($n = 3$ animals for each group; Non-D versus T2DM, $P < 0.001$, Watson U^2 test). Number of cilia (n) with an accessible tip within a 30 μm^2 area and high circular standard deviation (CSD) of the mean are indicated. (C-G) Prom-1 (C, D), Sox2 (E, F, G) and DCX (F, G) immunoreactivities in the lateral wall of Non-D, T1DM and T2DM brains were observed by bright field microscopy (C, E) and quantified along the predefined ROI (D, F, G). In parallel, Sox2 immunolabeling in the SVZ at 7 days after drug injections was performed and quantified. Note the presence of Prom-1 at the ciliary tips (green arrowheads, C) in Non-D and T1DM or its accumulation at the apical surface (red arrowheads, C) in T2DM. Numerous ciliary tufts in T2DM lack Prom-1 (asterisk, C). CP, caudoputamen; LV, lateral ventricle. Scale bars, (A) top panels, 10 μm; bottom panels, 5 μm; (C) left panel, 100 μm; right panels, 2 μm; (E) 50 μm. Data are presented as the mean ± SD. ***$P < 0.001$; ****$P < 0.0001$

decreased after one week of diabetes. Ongoing studies comparing the different glucose transporters in both diabetic models would probably help to understand these pathogenic mechanisms.

Interestingly, we also found that T2DM-impaired ependymal cilia lacked Prom-1 at their tips. Localized absence of this glycoprotein could be either a direct effect of the T2DM metabolic changes, or a secondary

effect of these conditions on the intraflagellar trafficking of membrane proteins (Bhogaraju et al., 2013). The presence of Prom-1 immunoreactivity in the apical cytoplasm of T2DM and T1DM ependymal cells is consistent with such intracellular trafficking impairment. Observations made 4 days after diabetogenic treatments also support dysfunction of intraflagellar transport in cilia as an early step in the neural deterioration of diabetic animals. Alternatively, but not exclusively, augmented release of small Prom-1^{+} membrane vesicles from cilia into the CSF, as previously demonstrated in murine embryonic neural progenitors (Marzesco et al., 2005), could explain the lack of Prom-1 in ciliary tips.

Prom-1 knockdown only induced a mild alteration of ependymal cilia in vivo. It did not alter the orientation of ciliary tufts as observed in T2DM, but cilia showed a tendency to clump together. Consistent with increased adhesiveness, numerous small protruding structures detected along the cilia of ependymal cells cultured in vitro suggested the attachment of extracellular vesicles, as has been described for biliary exosomes (Masyuk et al., 2010). Increased adhesiveness among Prom-1$^{-/-}$ ependymal cilia resembled the "stickiness" of rhabdomeric microvilli in *Drosophila* eyes lacking prominin (Zelhof et al., 2006), supporting involvement of this protein in the mechanisms underlying T2DM ciliary impairment.

It must be considered that cilia hold, at least, 300 different proteins. Furthermore, ciliary biogenesis and maintenance rely on a wealth of protein interactions and pathways comprising a recently estimated number of 1300 players (Boldt et al., 2016; van Dam et al., 2013). In this landscape, understanding the role of Prom-1 in the severe ciliary alterations driven by the early T2DM-like condition would require knowledge about every Prom-1 interaction with other ciliary proteins. Some of the identified Prom-1 interactions are nonetheless, instructive and might be relevant in our context. In the fruit fly eye, Prom interacts with spacemaker/eyeshut, a secreted EGF-like protein, which guides the spatial organization of compound eyes (Zelhof et al., 2006). In mammalian photoreceptors, Prom-1 interacts with protocadherin 21, forming a complex that is crucial for the architectural consolidation of the photoreceptor cell outer segment, which is a modified cilium (Gurudev et al., 2013; Yang et al., 2008). It remains to be determined which molecules could interact with Prom-1 in ependymal cilia. Potential candidates are cadherins Celsr2 and Celsr3; both containing multiple EGF-like domains, just like spacemaker/eyeshut. Knockdown of these cadherins determines ciliary phenotypes in ependymal cells similar to the T2DM changes described here, leading to lethal hydrocephalus (Tissir et al., 2010). These phenotypes have been associated to changes in the planar cell polarity pathway and the basal bodies (Tissir et al., 2010). Thus, a delocalization of Prom-1 contributing to increased tip adhesiveness, plus a derangement of basal bodies and other ciliary control molecules would be responsible for the alteration of ciliary architecture leading to the global disorientation of ciliary tufts.

The selective decrease of cell nuclei in the SVZ ependymal layer, together with the fall of neurogenesis and proliferation markers, suggests that T2DM animals suffered a rapid depletion of SVZ neural stem cells, intermediate progenitors and neuroblasts. Interestingly, in this model, DCX^{+} cells were present not only along the entire length of the RMS, but also frequently appeared in ectopic locations such as the corpus callosum, the caudoputamen and the olfactory peduncle. Considering that the normal beating of ependymal cilia provides directional cues for the proper migration of neuroblasts from the SVZ to the olfactory bulbs (Sawamoto et al., 2006), the ciliary defects observed in T2DM may likely contribute to ectopic neuroblast migration. The latter might also reflect damage of different brain targets, as has been described for the radial pathway through the corpus callosum (Castañeda et al., 2011; Goodus et al., 2015). Importantly, it has recently been demonstrated that traumatic brain injuries can be accompanied by reversible ependymal cilia defects, evidencing that recovery of diabetic ciliary impairment might be possible (Xiong et al., 2014).

That T2DM provoked a far more severe phenotype than T1DM seems to be in line with clinical studies showing that the risk for dementia is greater in T2DM than in T1DM (McCrimmon et al., 2012; Zilliox et al., 2016). Similar examples documented in the literature include the earlier appearance of peripheral neuropathy and nerve structural damage in the cornea of mouse under T2DM than under T1DM conditions (Yorek et al., 2015).

Is Prom-1 involved in diabetes? The implication of Prom-1 in cellular physiology has been investigated in several cellular systems and animal models. Especially, the effect of *Prom1* gene ablation has been addressed in different tissues (reviewed in Ref. (Fargeas et al., 2015)). In most models, mice were reported as viable and fertile, with a normal lifespan and no obvious abnormality other than a progressive photoreceptor degeneration leading to complete loss of vision (Dellett et al., 2014; Zacchigna et al., 2009). The latter observation is consistent with the role of Prom-1 in the organization of photoreceptor cell sensory cilia and mutations in human *PROM1* gene that cause various forms of retinal phenotypes, including macular degeneration or retinitis pigmentosa (Gurudev et al., 2013). Interestingly, one study has reported a mature obesity in another *Prom-1*$^{-/-}$ mouse line with ≈15% increase of body weight over 13-week period (Karim et al., 2014). Although we did not observe obesity at this early stage, our old knockout animals, specifically the males, showed an increased body weight after 20 weeks (EB, DC, unpublished data). Conceivably, different genetic backgrounds might modulate the permeability to metabolic disorders in *Prom-1* null mice. Although this issue waits to be explored, Prom-1 might emerge as a new player in disorders of energy metabolism involving membrane protrusions such as cilia (Oh et al., 2015).

Likewise, the impact of Prom-1 in neural system needs to be further dissected. Although no significant alterations were detected in the SVZ, other than a partial clumping of cilia (Zacchigna et al., 2009) (this study), a reduction in the number of new neurons surviving in the adult subgranular zone (SGZ), the second adult neurogenic niche, was previously described in our *Prom1* null mice (Walker et al., 2013). Given that Akt is a cell survival promoter, the interaction of Prom-1 with phosphoinositide 3-kinase (PI3K) and PI3K/Akt pathway (Wei et al., 2013) would deserve further attention in the SVZ and SGZ in T2DM model. Thus, Prom-1 may act not only as a scaffold protein involved in the organization of plasma membrane protrusion, but also as a central signaling regulator. Both functions might collectively link the role of Prom-1 on healthy and pathological conditions.

5. Conclusions

To our knowledge, this is the first study recognizing the early effect of diabetes on the SVZ. Most important, as shown by their presence before neurogenesis deterioration could be detected, ciliary defects appear as the primary event in the causal sequence of SVZ lesions. Therefore, as proposed by Gerdes et al. (2014), ciliary dysfunction would be at the root of T2DM pathogenesis.

Conflict of interests

The authors declare no conflict of interests.

Author contributions

AMS, DC and TPB were involved in the study concept and design, analyzed the data and wrote the manuscript. TPB performed in vivo experiments. JK designed, performed and analyzed in vitro experiments and contributed to the writing of the manuscript. EB, VB and MMR contributed to the histochemical studies performed in brain and pancreas, and analyzed the data. PC contributed to the generation of *Prom-1* null mice. All co-authors participated in the reading and revision of the manuscript.

Acknowledgments

We thank Fabián Tricárico from the SEM facility at the Museo Argentino de Ciencias Naturales (MACN, Buenos Aires), Guillermo Gastón from the School of Biomedical Sciences Animal House (Buenos Aires), Hella Hartmann from the Light Microscopy Facility and Thomas Kurth from the Electron Microscopy/Histology Facility at the BIOTEC (Dresden) for their skillful and dedicated technical assistance. We also thank Sylvi Graupner (BIOTEC) for the in vitro cell cultures. AMS and DC were supported by grants from Universidad Austral, Ministerio de Ciencia, Tecnología e Innovación Productiva (MINCyT) and the Bundesministerium für Bildung und Forschung (BMBF, 01DN13019/PRONEURAL). AMS, TPB and MMR were also supported by the Consejo Nacional de Investigaciones Científicas y Técnicas (CONICET) and Universidad Austral. DC was further supported by the Deutsche Forschungsgemeinschaft (DFG, SFB655-B3) and Sächsisches Staatsministerium für Wissenschaft und Kunst (4-7531.60/29/31). PC was supported by Longterm Structural Methusalem Funding of the Flemish Government, by EFSD/Novo Nordisk and by grants from the FWO (G.0209.07) - Fund for Scientific Research of the Flemish Government. The funders had no role in study design, data collection and analysis, decision to publish, or preparation of the manuscript.

Appendix A. Supplementary data

Supplementary data to this article can be found online at http://dx.doi.org/10.1016/j.nbd.2017.07.010.

References

Alvarez-Buylla, A., et al., 2008. The heterogeneity of adult neural stem cells and the emerging complexity of their niche. Cold Spring Harb. Symp. Quant. Biol. 73, 357–365.
Andrikopoulos, S., et al., 2008. Evaluating the glucose tolerance test in mice. Am. J. Physiol. Endocrinol. Metab. 295, E1323–32.
Bachor, T.P., Suburo, A.M., 2012. Neural stem cells in the diabetic brain. Stem Cells Int. 2012, 820790.
Bachor, T.P., et al., 2015. Sitagliptin protects proliferation of neural progenitor cells in diabetic mice. Metab. Brain Dis. 30, 885–893.
Beauquis, J., et al., 2006. Reduced hippocampal neurogenesis and number of hilar neurones in streptozotocin-induced diabetic mice: reversion by antidepressant treatment. Eur. J. Neurosci. 23, 1539–1546.
Bhogaraju, S., et al., 2013. Intraflagellar transport complex structure and cargo interactions. Cilia 2, 10.
Biessels, G.J., et al., 2014. Dementia and cognitive decline in type 2 diabetes and prediabetic stages: towards targeted interventions. Lancet Diabetes Endocrinol. 2, 246–255.
Boldt, K., et al., 2016. An organelle-specific protein landscape identifies novel diseases and molecular mechanisms. Nat. Commun. 7, 11491.
Castañeda, M.M., et al., 2010. Endothelinergic cells in the subependymal region of mice. Brain Res. 1321, 20–30.
Castañeda, M.M., et al., 2011. Endothelinergic signaling during recovery of brain cortical lesions. Neurol. Res. 33, 137–144.
Chatterjee, S., et al., 2016. Type 2 diabetes as a risk factor for dementia in women compared with men: a pooled analysis of 2.3 million people comprising more than 100,000 cases of dementia. Diabetes Care 39, 300–307.
Codega, P., et al., 2014. Prospective identification and purification of quiescent adult neural stem cells from their in vivo niche. Neuron 82, 545–559.
Corbeil, D., et al., 2001. Prominin: a story of cholesterol, plasma membrane protrusions and human pathology. Traffic 2, 82–91.
Coskun, V., et al., 2008. CD133 + neural stem cells in the ependyma of mammalian postnatal forebrain. Proc. Natl. Acad. Sci. U. S. A. 105, 1026–1031.
van Dam, T.J., et al., 2013. The SYSCILIA gold standard (SCGSv1) of known ciliary components and its applications within a systems biology consortium. Cilia 2, 7.
Del Bigio, M.R., 1995. The ependyma: a protective barrier between brain and cerebrospinal fluid. Glia 14, 1–13.
Delgehyr, N., et al., 2015. Ependymal cell differentiation, from monociliated to multiciliated cells. Methods Cell Biol. 127, 19–35.
Dellett, M., et al., 2014. Genetic background and light-dependent progression of photoreceptor cell degeneration in Prominin-1 knockout mice. Invest. Ophthalmol. Vis. Sci. 56, 164–176.
Doetsch, F., et al., 1999. Subventricular zone astrocytes are neural stem cells in the adult mammalian brain. Cell 97, 703–716.
Dubreuil, V., et al., 2007. Midbody and primary cilium of neural progenitors release extracellular membrane particles enriched in the stem cell marker prominin-1. J. Cell Biol. 176, 483–495.
van Duinkerken, E., et al., 2014. Ventral striatum, but not cortical volume loss, is related to cognitive dysfunction in type 1 diabetic patients with and without microangiopathy. Diabetes Care 37, 2483–2490.
Ernst, A., et al., 2014. Neurogenesis in the striatum of the adult human brain. Cell 156, 1072–1083.
Fargeas, C.A., et al., 2015. Commentary: "prom1 function in development, intestinal inflammation, and intestinal tumorigenesis". Front. Oncol. 5, 91.
Feliciano, D.M., et al., 2014. Embryonic cerebrospinal fluid nanovesicles carry evolutionarily conserved molecules and promote neural stem cell amplification. PLoS One 9, e88810.
Festa, A., et al., 2006. The natural course of beta-cell function in nondiabetic and diabetic individuals: the insulin resistance atherosclerosis study. Diabetes 55, 1114–1120.
Fliegauf, M., et al., 2007. When cilia go bad: cilia defects and ciliopathies. Nat. Rev. Mol. Cell Biol. 8, 880–893.
Garcia-Verdugo, J.M., et al., 1998. Architecture and cell types of the adult subventricular zone: in search of the stem cells. J. Neurobiol. 36, 234–248.
Gerdes, J.M., et al., 2014. Ciliary dysfunction impairs beta-cell insulin secretion and promotes development of type 2 diabetes in rodents. Nat. Commun. 5, 5308.
Goodus, M.T., et al., 2015. Neural stem cells in the immature, but not the mature, subventricular zone respond robustly to traumatic brain injury. Dev. Neurosci. 37, 29–42.
Gurudev, N., et al., 2013. Prominent role of prominin in the retina. Adv. Exp. Med. Biol. 777, 55–71.
Hu, F.B., et al., 2015. Curbing the diabetes pandemic: the need for global policy solutions. JAMA 313, 2319–2320.
Huttner, H.B., et al., 2008. The stem cell marker prominin-1/CD133 on membrane particles in human cerebrospinal fluid offers novel approaches for studying central nervous system disease. Stem Cells 26, 698–705.
Ishikawa, H., Marshall, W.F., 2017. Intraflagellar transport and ciliary dynamics. Cold Spring Harb. Perspect. Biol. 9, 1–13.
Karim, B.O., et al., 2014. Prom1 function in development, intestinal inflammation, and intestinal tumorigenesis. Front. Oncol. 4, 323.
Kim, J.H., et al., 2014. Diabetic characteristics and alveolar bone loss in streptozotocin- and streptozotocin-nicotinamide-treated rats with periodontitis. J. Periodontal Res. 49, 792–800.
Koizumi, H., et al., 2006. Doublecortin maintains bipolar shape and nuclear translocation during migration in the adult forebrain. Nat. Neurosci. 9, 779–786.
Liu, L., Duff, K., 2008. A technique for serial collection of cerebrospinal fluid from the cisterna magna in mouse. J. Vis. Exp. 21, 960.
Marzesco, A.M., et al., 2005. Release of extracellular membrane particles carrying the stem cell marker prominin-1 (CD133) from neural progenitors and other epithelial cells. J. Cell Sci. 118, 2849–2858.
Masyuk, A.I., et al., 2010. Biliary exosomes influence cholangiocyte regulatory mechanisms and proliferation through interaction with primary cilia. Am. J. Physiol. Gastrointest. Liver Physiol. 299, G990–9.
McCrimmon, R.J., et al., 2012. Diabetes and cognitive dysfunction. Lancet 379, 2291–2299.
Mirzadeh, Z., et al., 2008. Neural stem cells confer unique pinwheel architecture to the ventricular surface in neurogenic regions of the adult brain. Cell Stem Cell 3, 265–278.
Mullins, R.J., et al., 2017. Insulin resistance as a link between amyloid-beta and tau pathologies in Alzheimer's disease. Front. Aging Neurosci. 9, 118.
Nakamura, T., et al., 2006. Establishment and pathophysiological characterization of type 2 diabetic mouse model produced by streptozotocin and nicotinamide. Biol. Pharm. Bull. 29, 1167–1174.
NCD-RisC, 2016. Worldwide trends in diabetes since 1980: a pooled analysis of 751 population-based studies with 4.4 million participants. Lancet 387, 1513–1530.
Oh, E.C., et al., 2015. Metabolic regulation and energy homeostasis through the primary cilium. Cell Metab. 21, 21–31.
Ohata, S., Alvarez-Buylla, A., 2016. Planar organization of multiciliated ependymal (E1) cells in the brain ventricular epithelium. Trends Neurosci. 39, 543–551.
Ohn, J.H., et al., 2016. 10-year trajectory of beta-cell function and insulin sensitivity in the development of type 2 diabetes: a community-based prospective cohort study. Lancet Diabetes Endocrinol. 4, 27–34.
Paxinos, G., Franklin, K.B.J., 2001. The Mouse Brain in Stereotaxic Coordinates. Academic Press, San Diego.
Pevny, L.H., Nicolis, S.K., 2010. Sox2 roles in neural stem cells. Int. J. Biochem. Cell Biol. 42, 421–424.
Ramos-Rodriguez, J.J., et al., 2014. Central proliferation and neurogenesis is impaired in type 2 diabetes and prediabetes animal models. PLoS One 9, e89229.
Sartorius, T., et al., 2015. The brain response to peripheral insulin declines with age: a contribution of the blood-brain barrier? PLoS One 10, e0126804.
Sawamoto, K., et al., 2006. New neurons follow the flow of cerebrospinal fluid in the adult brain. Science 311, 629–632.
Schindelin, J., et al., 2012. Fiji: an open-source platform for biological-image analysis. Nat. Methods 9, 676–682.
Smolina, K., et al., 2015. Risk of dementia in patients hospitalised with type 1 and type 2 diabetes in England, 1998-2011: a retrospective national record linkage cohort study. Diabetologia 58, 942–950.
Tissir, F., et al., 2010. Lack of cadherins Celsr2 and Celsr3 impairs ependymal ciliogenesis, leading to fatal hydrocephalus. Nat. Neurosci. 13, 700–707.
Tran, P.V., et al., 2008. THM1 negatively modulates mouse sonic hedgehog signal transduction and affects retrograde intraflagellar transport in cilia. Nat. Genet. 40, 403–410.
Walker, T.L., et al., 2013. Prominin-1 allows prospective isolation of neural stem cells from the adult murine hippocampus. J. Neurosci. 33, 3010–3024.

Wei, Y., et al., 2013. Activation of PI3K/Akt pathway by CD133-p85 interaction promotes tumorigenic capacity of glioma stem cells. Proc. Natl. Acad. Sci. U. S. A. 110, 6829–6834.
Weigmann, A., et al., 1997. Prominin, a novel microvilli-specific polytopic membrane protein of the apical surface of epithelial cells, is targeted to plasmalemmal protrusions of non-epithelial cells. Proc. Natl. Acad. Sci. U. S. A. 94, 12425–12430.
Xiong, G., et al., 2014. Traumatic brain injury-induced ependymal ciliary loss decreases cerebral spinal fluid flow. J. Neurotrauma 31, 1396–1404.
Yang, Z., et al., 2008. Mutant prominin 1 found in patients with macular degeneration disrupts photoreceptor disk morphogenesis in mice. J. Clin. Invest. 118, 2908–2916.
Yang, S., et al., 2015. Impaired macromolecular protein pools in fronto-striato-thalamic circuits in type 2 diabetes revealed by magnetization transfer imaging. Diabetes 64, 183–192.
Yorek, M.S., et al., 2015. Effect of diet-induced obesity or type 1 or type 2 diabetes on corneal nerves and peripheral neuropathy in C57Bl/6J mice. J. Peripher. Nerv. Syst. 20, 24–31.
Zacchigna, S., et al., 2009. Loss of the cholesterol-binding protein prominin-1/CD133 causes disk dysmorphogenesis and photoreceptor degeneration. J. Neurosci. 29, 2297–2308.
Zelhof, A.C., et al., 2006. Transforming the architecture of compound eyes. Nature 443, 696–699.
Zhang, W.J., et al., 2008. Impairment of hippocampal neurogenesis in streptozotocin-treated diabetic rats. Acta Neurol. Scand. 117, 205–210.
Zhao, C., et al., 2008. Mechanisms and functional implications of adult neurogenesis. Cell 132, 645–660.
Ziegler, A.N., et al., 2015. Insulin and IGF receptor signalling in neural-stem-cell homeostasis. Nat. Rev. Endocrinol. 11, 161–170.
Zilliox, L.A., et al., 2016. Diabetes and cognitive impairment. Curr. Diab. Rep. 16, 87.